AMERICAN SOCIETY FOR MICROBIOLOGY | Journal of Virology®

VIRUS-CELL INTERACTIONS

Role of the Orphan Transporter SLC35E1 in the Nuclear Egress of Herpes Simplex Virus 1

Fumio Maeda,[a,b,h] Akihisa Kato,[a,b,c] Kosuke Takeshima,[a,b] Misato Shibazaki,[a,b] Ryota Sato,[d] Takuma Shibata,[d] Kensuke Miyake,[d] Hiroko Kozuka-Hata,[e] Masaaki Oyama,[e] Eigo Shimizu,[f] Seiya Imoto,[g] Satoru Miyano,[f] Shungo Adachi,[h] Tohru Natsume,[h] Koh Takeuchi,[h] Yuhei Maruzuru,[a,b,c] Naoto Koyanagi,[a,b,c] Arii Jun,[a,b,c] Kawaguchi Yasushi[a,b,c]

[a]Division of Molecular Virology, Department of Microbiology and Immunology, The Institute of Medical Science, The University of Tokyo, Tokyo, Japan
[b]Department of Infectious Disease Control, International Research Center for Infectious Diseases, The Institute of Medical Science, The University of Tokyo, Tokyo, Japan
[c]Research Center for Asian Infectious Diseases, The Institute of Medical Science, The University of Tokyo, Tokyo, Japan
[d]Division of Innate Immunity, Department of Microbiology and Immunology, The Institute of Medical Science, The University of Tokyo, Tokyo, Japan
[e]Medical Proteomics Laboratory, The Institute of Medical Science, The University of Tokyo, Tokyo, Japan
[f]Laboratory DNA Information Analysis, Human Genome Center, The Institute of Medical Science, The University of Tokyo, Tokyo, Japan
[g]Laboratory Health Medical Intelligence, Human Genome Center, The Institute of Medical Science, The University of Tokyo, Tokyo, Japan
[h]Cellular and Molecular Biotechnology Research Institute, National Institute of Advanced Industrial Science and Technology, Tokyo, Japan

ABSTRACT This study developed a system consisting of two rounds of screening cellular proteins involved in the nuclear egress of herpes simplex virus 1 (HSV-1). Using this system, we first screened cellular proteins that interacted with the HSV-1 nuclear egress complex (NEC) consisting of UL34 and UL31 in HSV-1-infected cells, which are critical for the nuclear egress of HSV-1, by tandem affinity purification coupled with mass spectrometry-based proteomics technology. Next, we performed CRISPR/Cas9-based screening of live HSV-1-infected reporter cells under fluorescence microscopy using single guide RNAs targeting the cellular proteins identified in the first proteomic screening to detect the mislocalization of the lamin-associated protein emerin, which is a phenotype for defects in HSV-1 nuclear egress. This study focused on a cellular orphan transporter SLC35E1, one of the cellular proteins identified by the screening system. Knockout of SLC35E1 reduced HSV-1 replication and induced membranous invaginations containing perinuclear enveloped virions (PEVs) adjacent to the nuclear membrane (NM), aberrant accumulation of PEVs in the perinuclear space between the inner and outer NMs and the invagination structures, and mislocalization of the NEC. These effects were similar to those of previously reported mutation(s) in HSV-1 proteins and depletion of cellular proteins that are important for HSV-1 de-envelopment, one of the steps required for HSV-1 nuclear egress. Our newly established screening system enabled us to identify a novel cellular protein required for efficient HSV-1 de-envelopment.

IMPORTANCE The identification of cellular protein(s) that interact with viral effector proteins and function in important viral procedures is necessary for enhancing our understanding of the mechanics of various viral processes. In this study, we established a new system consisting of interactome screening for the herpes simplex virus 1 (HSV-1) nuclear egress complex (NEC), followed by loss-of-function screening to target the identified putative NEC-interacting cellular proteins to detect a defect in HSV-1 nuclear egress. This newly established system identified SLC35E1, an orphan transporter, as a novel cellular protein required for efficient HSV-1 de-envelopment, providing an insight into the mechanisms involved in this viral procedure.

KEYWORDS HSV-1, SLC35E1, transporter, nuclear egress

Editor Rozanne M. Sandri-Goldin, University of California, Irvine

Address correspondence to Kawaguchi Yasushi, ykawagu@ims.u-tokyo.ac.jp.

The authors declare no conflict of interest.

Received 21 February 2022
Accepted 21 February 2022
Published 27 April 2022

Herpesviruses replicate their genomes, and nascent progeny viral genomes are packaged into capsids in the nucleus (1–3). Then, the genome-containing nucleocapsids in the nucleus are transported to the cytoplasm where they acquire a final envelope to produce infectious virions (3–6). The nascent nucleocapsids are then exported from the nucleus by a sequential envelopment-de-envelopment process termed nuclear egress (3–6). The nucleocapsids acquire a primary envelope by budding through the inner nuclear membrane (INM) into the perinuclear space between the INM and the outer nuclear membrane (ONM) (primary envelopment). Fusion between the perinuclear enveloped virions (PEVs) and the ONM allows the release of nucleocapsids into the cytoplasm (de-envelopment). Primary envelopment requires several steps, including nuclear lamina disruption, nucleocapsid docking to the INM, incorporation of nucleocapsids into INM-derived vesicles (PEVs), deformation of the INM around the nucleocapsid, which creates a nascent bud, and scission of the INM that finally releases PEVs into the perinuclear space (3–6). Most of these processes are thought to be mediated by the heterodimeric nuclear egress complex (NEC), which consists of two viral proteins that are conserved among members of the family *Herpesviridae* (3–6). The NEC of herpes simplex virus 1 (HSV-1), subclassified into the *Alphaherpesvirinae* subfamily of the *Herpesviridae* family, consists of UL34 and UL31 (3–6). The NEC is thought to be important for the membrane deformation step of primary envelopment because HSV-1 NEC and its homolog, porcine alphaherpesvirus pseudorabies virus, can directly vesiculate membranes *in vitro* (7–11). Furthermore, the HSV-1 NEC is thought to exhibit multifunctionality during nuclear egress by interacting with cellular and other viral proteins. First, to allow nucleocapsid docking at the INM, the nuclear lamina, a dense filamentous network underneath the INM primarily composed of lamins (12), which is an obstacle for nucleocapsids, must be dissolved. In normal cells, the lamina is disassembled by the phosphorylation of lamins and lamin-associated proteins (LAPs) mediated by cellular protein kinases, including protein kinase C (PKC), during mitosis (12). In HSV-1-infected cells, HSV-1 protein kinase Us3 phosphorylates lamins and LAPs (13–17), and PKC is recruited to the INM by a mechanism dependent on the NEC and HSV-1 ICP34.5 (18, 19). The NEC interacts with PKC, lamins, Us3, and ICP34.5, and these interactions are thought to mediate the disruption of the nuclear lamina by altering the phosphorylation status of the lamins and LAPs (13, 15, 18–26). Second, the NEC binds directly to UL25, a component of the capsid vertex-specific complex, which allows the incorporation of the nucleocapsid into the PEVs (27–29). Third, the NEC interacts with ALIX, an ESCRT-III adaptor, which recruits ESCRT-III machinery to the INM via ALIX for the efficient scission of the INM during primary envelopment (6, 30). Fourth, the HSV-1 proteins Us3, gB, gH, UL47, and ICP22 and cellular proteins CD98 heavy chain (CD98hc), β-integrin, and p32 interact with the NEC and promote the efficient de-envelopment and/or primary envelopment, although the mechanisms involved are poorly understood (22, 23, 31–37). It has also been reported that UL21 proteins of HSV-1 and -2 are involved in viral de-envelopment (38). Furthermore, cellular proteins, including the torsins, protein kinase D and its regulators, vesicle-associated membrane protein-associated protein B, and Tsg101, were reported to be involved in nuclear egress, although the interactions of these cellular proteins with the NEC remain to be determined (39–42). Thus, in addition to HSV-1 NEC, other cellular and viral proteins might participate during the various steps of HSV-1 nuclear egress. Taken together, it appears that additional cellular and viral proteins are involved in HSV-1 nuclear egress, and a further understanding of this procedure will require their identification.

In this study, we screened host cell proteins in HSV-1-infected cells that interacted with the UL34 and UL31 complex by tandem affinity purification coupled with mass spectrometry-based proteomics technology. Then, we established an experimental system to detect a defect in HSV-1 nuclear egress in live infected reporter cells by fluorescence microscopy followed by CRISPR/Cas9-based functional screening using single guide RNAs (sgRNAs) targeting the cellular proteins identified in the first proteomic

screening. After two rounds of screening, we focused on SLC35E1, a cellular orphan transporter, and investigated its role in the nuclear egress of HSV-1.

RESULTS

Identification of cellular proteins that interact with the UL34 and UL31 complex in HSV-1-infected cells. To identify host cellular proteins that interacted with the UL34 and UL31 complex in HSV-1-infected cells, we constructed a recombinant virus YK742 (SE-UL34/Flag-UL31) encoding UL34 fused to tandem strep epitopes-tobacco etch virus (TEV) protease cleavage site (SE-UL34) (30) and UL31 fused to a Flag epitope tag (Flag-UL31) (Fig. 1A). Vero cells infected with YK742 (SE-UL34/Flag-UL31) produced SE-UL34 and Flag-UL31 at levels similar to those of UL34 and UL31, respectively, in Vero cells infected with wild-type HSV-1(F) (Fig. 1B), and the growth of YK742 (SE-UL34/Flag-UL31) in these cells was comparable with that of wild-type HSV-1(F) (Fig. 1C).

HaCaT cells were infected with YK742 (SE-UL34/Flag-UL31), lysed, precipitated twice with Strep-Tactin, reacted with anti-Flag M2 affinity gel, and subjected to mass spectrometry (Fig. 1D). These experiments identified 850 cell proteins and 58 viral proteins that precipitated with the UL34 and UL31 complex, including Us3, gB, gH, gD, UL47, UL25, p32, emerin, lamin A/C, lamin B1, importin subunit β-1, and SERCA2, which were previously reported to interact with the NECs of HSV-1 and a betaherpesvirus human cytomegalovirus (15, 22, 26–29, 33, 34, 43, 44).

Establishment of an experimental system to detect a defect in HSV-1 nuclear egress from live infected cells. Next, we established an experimental system to detect a defect in HSV-1 nuclear egress, which is applicable for CRISPR/Cas9-based loss-of-function screening. The HSV-1 Us3 protein kinase was reported to function in primary envelopment and de-envelopment (13–15, 31, 32, 36, 45). Mutations in Us3 cause striking phenotypes, including mislocalization of the NEC and emerin, a LAP, to discrete punctate structures around the NM, detected by fluorescence microscopy (46), and the induction of membranous structures that aberrantly accumulate PEVs, which were formed by invaginations of the INM into the nucleoplasm, detected at the ultrastructural level (16, 25, 31). Therefore, we generated HeLa cells stably expressing emerin fused to a monomeric fluorescence protein VenusA206K (47) (emerin-VenusA206K) with the inducible expression of Cas9 controlled by doxycycline treatment (HeLa/tet-on Cas9/emerin-VenusA206K cells) (Fig. 2A). In agreement with earlier reports (16, 25), HeLa/tet-on Cas9/emerin-VenusA206K cells infected with the Us3 kinase-dead mutant YK511 (Us3K220M) (48) showed discrete punctate structures of emerin-VenusA206K adjacent to the nuclear rim, which were well colocalized with those of UL34 (Fig. 2B). In contrast, emerin-VenusA206K and UL34 showed smooth colocalization along the nuclear rim in HeLa/tet-on Cas9/emerin-VenusA206K cells infected with wild-type HSV-1(F) (Fig. 2B). The punctate structures of emerin-VenusA206K adjacent to the nuclear rim and the smooth distribution of emerin-VenusA206K along the nuclear rim were also observed in living HeLa/tet-on Cas9/emerin-VenusA206K cells infected with YK511 (Us3K220M) or wild-type HSV-1(F), respectively (data not shown). Thus, our experimental system can detect the phenotypes of Us3 mutations in live HSV-1-infected cells under fluorescence microscopy, which can be used for CRISPR/Cas9-based screening.

CRISPER/Cas9-based screening to identify cellular proteins whose depletion induces punctate structures of emerin-VenusA206K around the nuclear rim in HSV-1-infected cells. We excluded 112 ribosomal and histone proteins from the 850 host cell proteins identified as putative NEC-interacting proteins in the first proteomic screening described above. Therefore, we introduced 10 sgRNAs for each of the 738 host cell proteins into HeLa/tet-on Cas9/emerin-VenusA206K cells with a lentivirus vector expressing blue fluorescence protein (BFP) in the presence of doxycycline to induce Cas9 expression (Fig. 3A). Then, we isolated BFP-positive cells by cell sorting and infected the lentivirus-transduced cells with wild-type HSV-1(F), screened cell clones with punctate structures of emerin-VenusA206K around the nuclear rim upon HSV-1(F) infection, and isolated 6 cell clones showing the expected phenotype and determined guide RNA sequences from the cell clones (Fig. 3B). Finally, we identified 6 host cellular

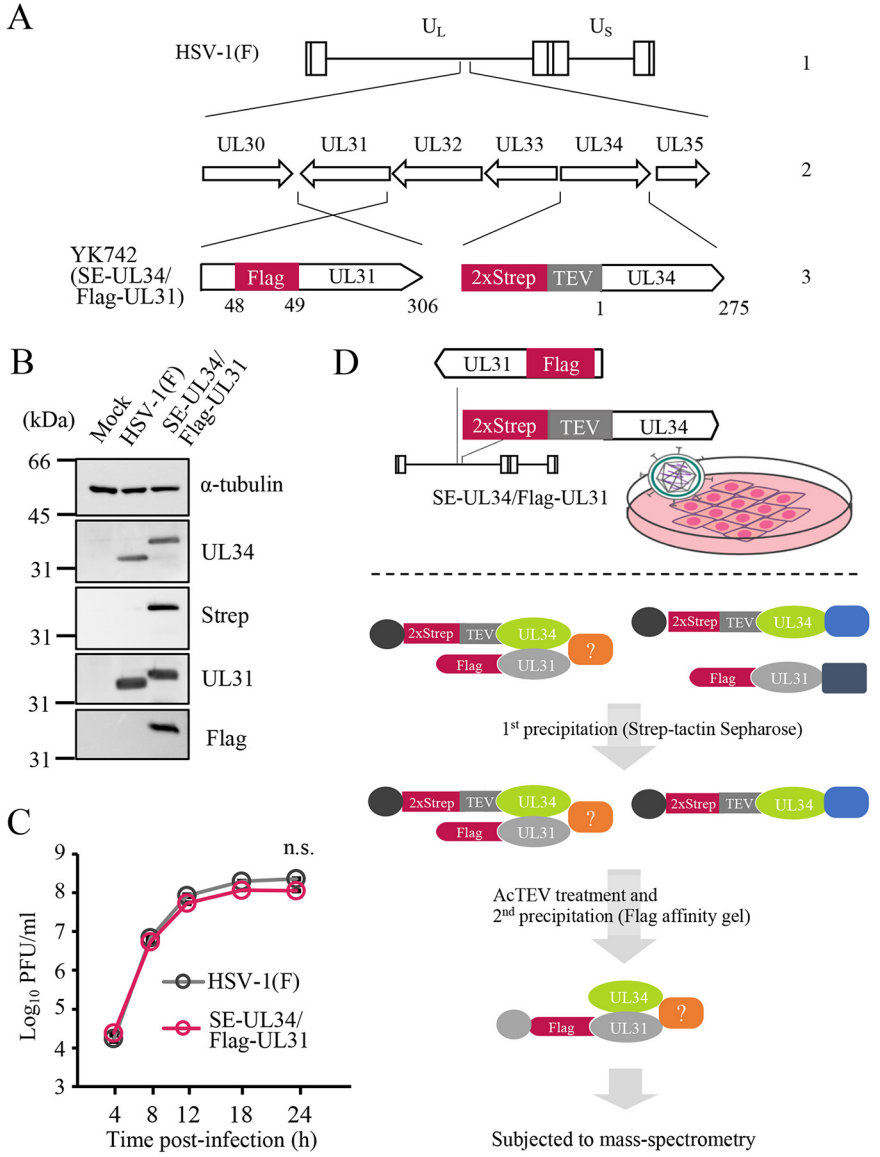

FIG 1 Characterization of a recombinant virus YK742 (SE-UL34/Flag-UL31) generated in this study and identification of proteins that interact with the complex of HSV-1 UL34 and UL31. (A) Line 1, wild-type HSV-1(F) genome; line 2, domains of UL30 to UL35; line 3, recombinant virus encoding UL34 fused with tandem strep epitopes (2xStrep)-TEV cleavage site and UL31 tagged with Flag epitope. (B) Vero cells mock infected or infected with wild-type HSV-1(F) or YK742 (SE-UL34/Flag-UL31) at an MOI of 5 for 18 h were analyzed by immunoblotting with the indicated antibodies. (C) Vero cells were infected with wild-type HSV-1(F) or YK742 (SE-UL34/Flag-UL31) at an MOI of 5. Total virus from the cell culture supernatants and infected cells was harvested and assayed on Vero cells. Each data point is the mean ± standard error of 3 independent experiments. Statistical analysis was performed by Student's *t* test. n.s., not significant. (D) Tandem affinity purification coupled with mass spectrometry-based proteomics to identify proteins that interact with the HSV-1 UL34 and UL31 complex in HSV-1-infected cells. HaCaT cells were infected with YK742 (SE-UL34/Flag-UL31) at an MOI of 5 for 24 h and lysed. After centrifugation, the supernatants were precipitated with Strep-Tactin Sepharose (1st precipitation). After treatment with AcTEV protease, the supernatants were immunoprecipitated with an anti-flag M2 affinity gel (2nd precipitation). Proteins with the tandem affinity purification were subjected to mass spectrometry.

proteins that were targeted by the determined sgRNAs (Table 1). Of these, only SLC35E1, a member of solute carrier family 35, was detected in two independent cell clones (Table 1). Therefore, we focused on this host cellular protein and investigated its role in HSV-1 nuclear egress further.

Interaction between SLC35E1 and UL34 in HSV-1-infected cells. To investigate the interaction between SLC35E1 and UL34 in HSV-1-infected cells, we generated HeLa

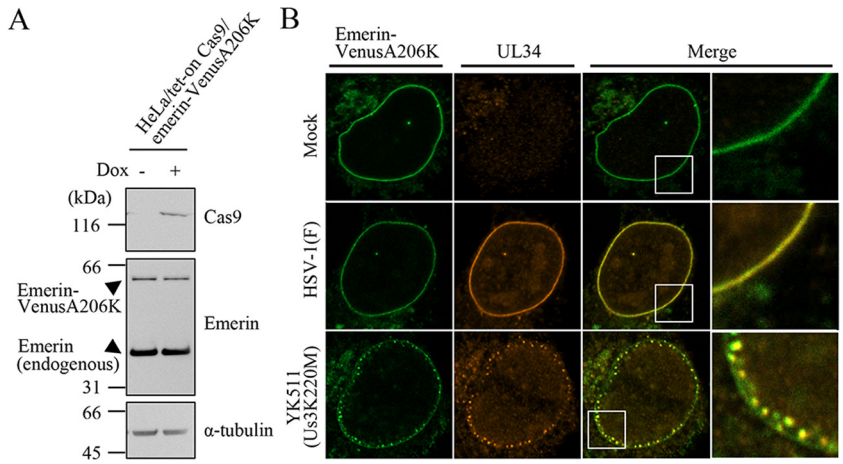

FIG 2 Characterization of HeLa/tet-on Cas9/emerin-VenusA206K cells. (A) HeLa/tet-on Cas9/emerin-VenusA206K cells mock treated or treated with 1 μg/mL of doxycycline (Dox) for 18 h were analyzed by immunoblotting with the indicated antibodies. (B) HeLa/tet-on Cas9/emerin-VenusA206K were mock infected or infected with wild-type HSV-1(F) or YK511 (Us3K220M) at an MOI of 5, fixed at 22 h postinfection, permeabilized, stained with anti-UL34 antibody, and examined by confocal microscopy.

cells ectopically expressing SLC35E1 (HeLa/SLC35E1 cells) and control HeLa/puro cells by the transduction of HeLa cells with a retrovirus vector expressing SLC35E1 or an empty retrovirus vector, respectively. As shown in Fig. 4A, an increase in SLC35E1 accumulation in HeLa/SLC35E1 cells was observed compared with that in HeLa/puro cells. HeLa/SLC35E1 cells were then infected with YK742 (SE-UL34/Flag-UL31) and lysed and precipitated with Strep-Tactin, and the precipitates were analyzed by immunoblotting. As shown in Fig. 4B, Strep-Tactin coprecipitated SLC35E1 and Flag-UL31 but not UL50 with SE-UL34 from lysates of YK742 (SE-UL34/Flag-UL31)-infected cells. In contrast, Strep-Tactin barely precipitated any of these viral and cellular proteins from lysates of wild-type HSV-1(F)-infected cells (Fig. 4B). These results indicated that UL34 formed a complex(es) with SLC35E1 and/or UL31 in HSV-1-infected cells, verifying the interaction data obtained by mass spectrometry-based proteomic screening.

Characterization of SLC35E1 knockout HeLa cells. To examine the effects of SLC35E1 in HSV-1-infected cells, we generated SLC35E1 knockout (KO) HeLa (HeLa/ΔSLC35E1) cells using the CRISPR/Cas9 system. To examine the off-target effects of SLC35E1 KO by the CRISPR/Cas9 system, we generated HeLa/ΔSLC35E1/SLC35E1 cells ectopically expressing SLC35E1 in HeLa/ΔSLC35E1 cells and control HeLa/ΔSLC35E1/puro cells by the transduction of HeLa/ΔSLC35E1 cells with a retrovirus vector expressing SLC35E1 or an empty retrovirus vector, respectively (30). In addition, other control HeLa/puro cells were generated by the transduction of HeLa cells with the empty retrovirus vector. The genotype analysis of HeLa/ΔSLC35E1 cells showed that different null mutations were introduced into the 4 SLC35E1 alleles (Fig. 5A).

The expression of SLC35E1 in HeLa/puro, HeLa ΔSLC35E1/puro, and HeLa/ΔSLC35E1/SLC35E1 cells that were mock infected or infected with wild-type HSV-1(F) for 22 h was analyzed by immunoblotting. As shown in Fig. 5B, the low but consistent expression of SLC35E1 was detected in mock- or HSV-1(F)-infected HeLa/puro cells. As expected, the expression of SLC35E1 was not detected in mock-infected or HSV-1(F)-infected HeLa/ΔSLC35E1/puro cells (Fig. 5B). Mock- or HSV-1(F)-infected HeLa/ΔSLC35E1/SLC35E1 cells expressed SLC35E1 efficiently, and, of note, the levels of SLC35E1 expression in these infected cells were higher than those of endogenous SLC35E1 expression in infected HeLa/puro cells (Fig. 5B). The viability of HeLa/ΔSLC35E1/puro cells was similar to that of HeLa/puro and HeLa/ΔSLC35E1/SLC35E1 cells (Fig. 5C).

Effect of SLC35E1 on the localization of UL34 in HSV-1-infected cells and on HSV-1 virion morphogenesis. HeLa/puro, HeLa/ΔSLC35E1/puro, and HeLa/ΔSLC35E1/SLC35E1 cells were infected with wild-type HSV-1(F) for 22 h, and the localization of UL34 in these infected cells was analyzed by confocal microscopy. As shown in Fig. 6,

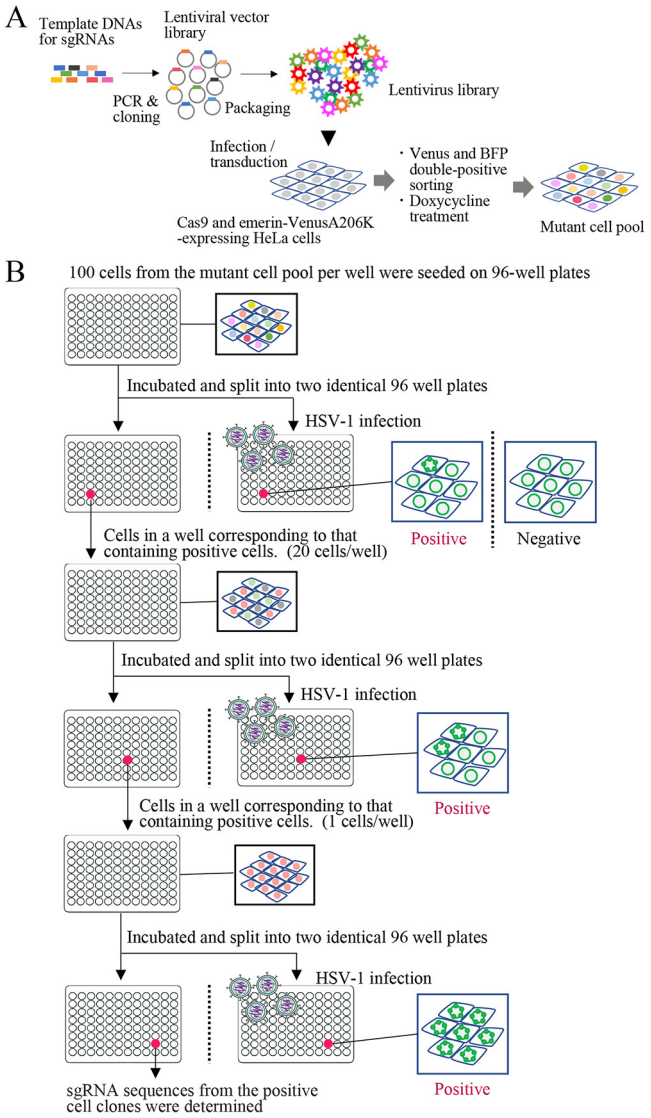

FIG 3 CRISPR/Cas9-based loss-of-function screening to detect the mislocalization of emerin-VenusA206K in live HSV-1-infected cells. (A) Template DNAs for sgRNAs (10 sgRNAs against each of the 738 cellular genes whose products were identified as putative NEC-interacting proteins by the interactome screening shown in Fig. 1D) were synthesized, amplified by PCR, and cloned into a lentivirus vector. HEK293FT cells were transfected with the resultant lentivirus vector library to generate lentivirus sgRNA library. HeLa/tet-on Cas9/emerin-VenusA206K cells were transduced with the lentivirus sgRNA library, and VenusA206K and BFP double-positive cell populations were sorted and left in the presence of doxycycline to generate a mutant cell pool. (B) One hundred cells from the mutant cell pool per well were seeded onto 96-well plates, incubated, and split into two identical 96-well plates. Cells on one plate were infected with wild-type HSV-1(F) and analyzed to detect aberrant punctate structures of emerin-VenusA206K adjacent to the NM by fluorescence microscopy. When punctate structures of emerin-VenusA206K were detected, cells on the corresponding well in another plate were seeded onto new 96-well plates (20 cells per well), incubated, split into two identical 96-well plates, and analyzed as described above. These processes were repeated until cell clones showing the punctate structures of emerin-VenusA206K in the presence of HSV-1 infection were isolated. Finally, sgRNA sequences from the positive cell clones were determined.

most (82%) of the infected HeLa/ΔSLC35E1/puro cells exhibited aberrant punctate structures of UL34 around the nuclear rim and in the nucleus, and there was a significantly higher frequency of UL34 punctate structures in infected HeLa/ΔSLC35E1/puro cells than infected HeLa/puro or HeLa/ΔSLC35E1/SLC35E1 cells. The punctate structures of UL34 were reminiscent of those of the NEC induced by Us3 mutations and the depletion of cellular effectors involved in HSV-1 nuclear egress, including CD98hc,

TABLE 1 List of genes determined by CRISPR/Cas9 screening

Clone no.	Gene ID[a]	Gene designation	Full name
1	10466	COG5	Conserved oligomeric Golgi complex subunit 5
1	23788	MTCH2	Mitochondrial carrier homolog 2
2	5718	PSMD12	26S proteasome non-ATPase regulatory subunit 12
3	10250	SRRM1	Serine arginine repetitive matrix protein 1
4	6427	SRSF2	Serine/arginine-rich splicing factor 2
5	79939	SLC35E1	Solute carrier family 35 member E1
6	79939	SLC35E1	Solute carrier family 35 member E1

[a]ID, identifier.

β1-integrin, and p32 (32–34, 36, 37, 46). These results suggested that SLC35E1 was required for the proper localization of the NEC in HSV-1-infected cells.

To examine the effects of SLC35E1 in HSV-1-infected cells at the ultrastructural level, HeLa/puro, HeLa/ΔSLC35E1/puro, and HeLa/ΔSLC35E1/SLC35E1 cells infected with wild-type HSV-1(F) for 22 h were subjected to electron microscopy, and viral morphogenesis was analyzed by quantitating the number of virus particles at different morphogenetic stages in these infected cells. As shown in Fig. 7A and Table 2, membranous invagination structures containing PEVs were readily observed adjacent to the NM in infected HeLa/ΔSLC35E1/puro cells. In contrast, these structures were not as frequent in infected HeLa/puro or HeLa/ΔSLC35E1/SLC35E1 cells (Fig. 7 and Table 2). The quantitation of these data showed 5- or 4-fold increases in membranous invagination structures in infected HeLa/ΔSLC35E1/puro cells compared with HeLa/puro or HeLa/ΔSLC35E1/SLC35E1 cells, respectively (Table 2). In infected HeLa/puro or HeLa/ΔSLC35E1/SLC35E1 cells, 4.0% and

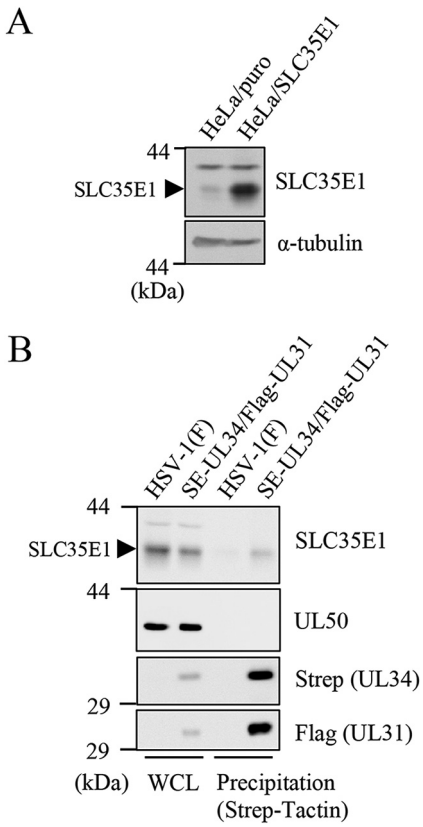

FIG 4 Coprecipitation of SLC35E1 with HSV-1 UL34 in HSV-1-infected cells. (A) HeLa/puro or HeLa/SLC35E1 cells were analyzed by immunoblotting with the indicated antibodies. (B) HeLa/SLC35E1 cells infected with wild-type HSV-1(F) or YK742 (SE-UL34/Flag-UL31) at an MOI of 5 for 22 h were harvested, precipitated with Strep-Tactin Sepharose, and analyzed by immunoblotting with indicated antibodies. WCL, whole-cell lysate.

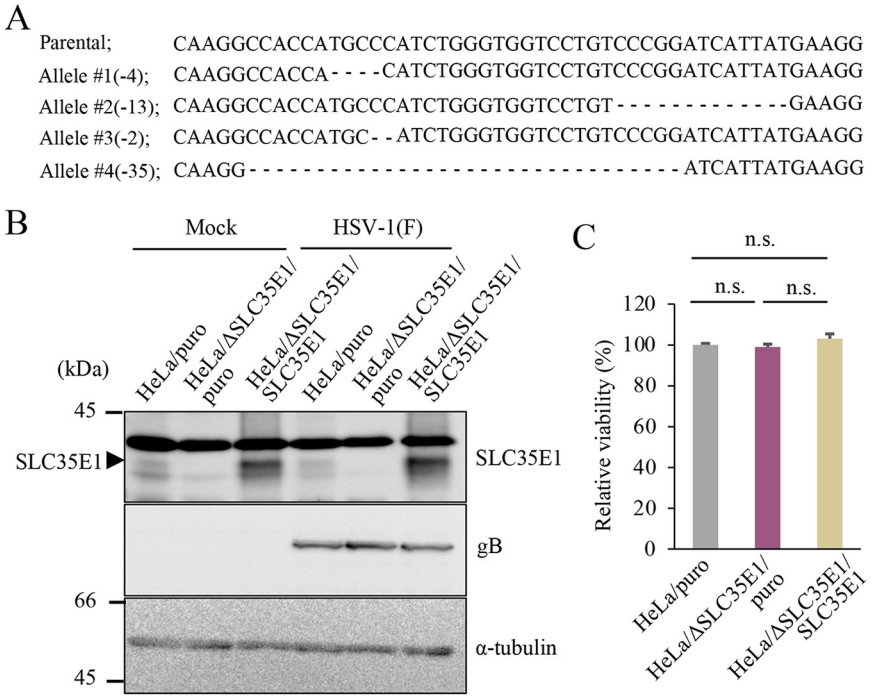

FIG 5 Characterization of HeLa/ΔSLC35E1/puro and HeLa/ΔSLC35E1/SLC35E1 cells. (A) The targeted SLC35E1 mutation sequences and the parental sequence in HeLa/ΔSLC35E1 cells that are parental cells of HeLa/ΔSLC35E1/puro and HeLa/ΔSLC35E1/SLC35E1 cells. (B) HeLa/puro, HeLa/ΔSLC35E1/puro, and HeLa/ΔSLC35E1/SLC35E1 cells were mock infected or infected with wild-type HSV-1(F) at an MOI of 5 for 22 h and analyzed by immunoblotting with the indicated antibodies. (C) Viability of HeLa/puro, HeLa/ΔSLC35E1/puro, and HeLa/ΔSLC35E1/SLC35E1 cells. Data are shown as the means ± standard error of the results of 3 independent experiments and are expressed relative to the mean determined for HeLa/puro cells, which was normalized to 100%. n.s., not significant. Statistical analysis was performed by one-way analysis of variance (ANOVA) and Tukey's test.

4.3% of the total number of virus particles were PEVs in the perinuclear space and invagination structures, respectively (Fig. 7B and Table 2). In contrast, the percentage of total virus particles in the perinuclear space and invagination structures in infected HeLa/ΔSLC35E1/puro cells was significantly increased to 19% (Fig. 7B and Table 2). This represented 4.8- and 4.4-fold increases compared with infected HeLa/puro or HeLa/ΔSLC35E1/SLC35E1 cells, respectively (Fig. 7B and Table 2). These results indicated that the SLC35E1 KO induced membranous invagination structures containing PEVs and the aberrant accumulation of PEVs in the perinuclear space and invagination structures.

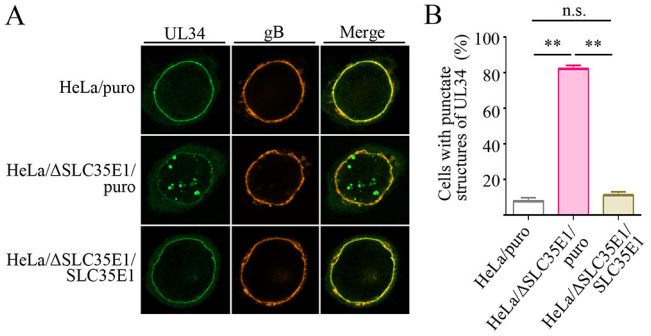

FIG 6 Effects of SLC35E1 KO on the localization of UL34 in HSV-1-infected cells. (A) HeLa/puro, ΔSLC35E1/puro, and ΔSLC35E1/SLC35E1 cells were infected with wild-type HSV-1(F) at an MOI of 5 for 22 h, stained with anti-UL34 and anti-gB antibodies, and examined by confocal microscopy. (B) Percentage of cells with aberrant punctate structures at the nuclear rim and in the nucleus was determined. Data are shown as the mean ± standard error of three independent experiments. Statistical analysis was performed by one-way ANOVA and Tukey's test. **, $P < 0.01$; n.s., not significant.

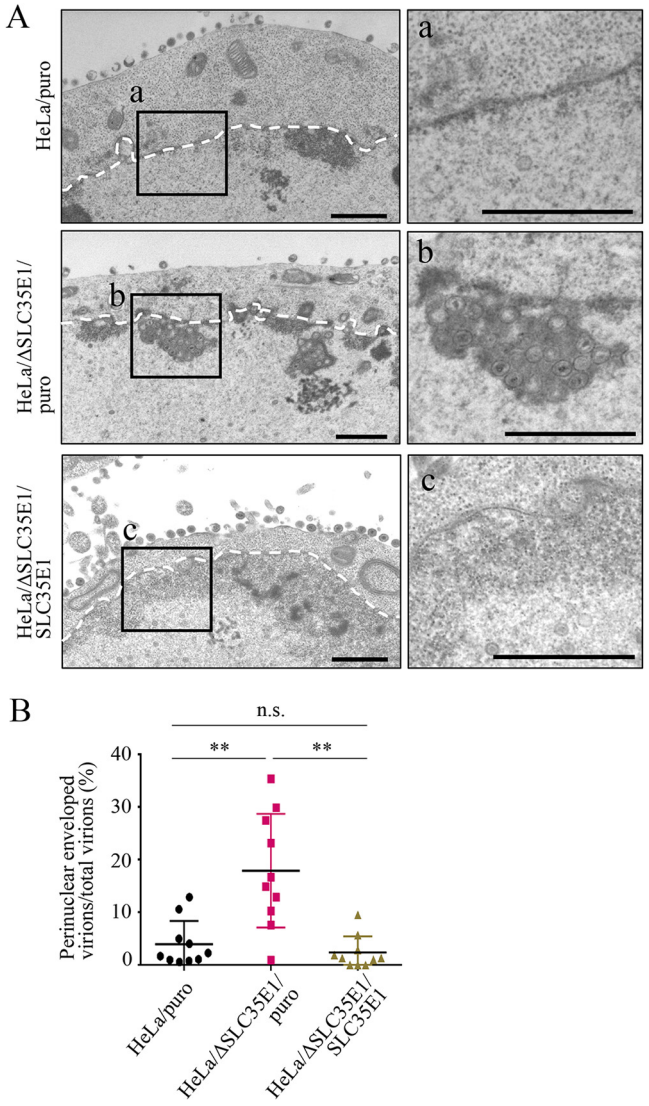

FIG 7 Effect of SLC35E1 KO on HSV-1 nuclear egress. (A) HeLa/puro, HeLa/ΔSLC35E1/puro, and HeLa/ΔSLC35E1/SLC35E1 cells were infected with wild-type HSV-1(F) at an MOI of 20, fixed at 22 h postinfection, embedded, sectioned, stained, and examined by transmission electron microscopy. The images labeled a to c on the right are magnifications of the corresponding boxed areas on the left. Bars, 1 μm. Dotted lines indicate the nuclear membrane. (B) Mean proportions of enveloped virions in the perinuclear space of 10 infected cells were determined. Statistical analysis was performed by one-way ANOVA with Turkey's test. **, $P < 0.01$; n.s., not significant.

Collectively, SLC35E1 KO exhibited phenotypes similar to those induced by the depletion and/or mutations in cellular and viral effectors involved in HSV-1 nuclear egress, including CD98hc, β1-integrin, p32, Us3, gB, and gH, with respect to the mislocalization of UL34 to the punctate structures, induction of membranous invagination structures containing PEVs adjacent to the NM, and aberrant accumulation of PEVs in the perinuclear space and invagination structures. These results suggested that SLC35E1 has a similar role to CD98hc, β1-integrin, p32, Us3, gB, and gH during HSV-1 nuclear egress.

Effect of SLC35E1 on HSV-1 replication in cell cultures. To examine the effect of SLC35E1 on HSV-1 replication in cell cultures, HeLa/puro, HeLa/ΔSLC35E1/puro, and HeLa/ΔSLC35E1/SLC35E1 cells were infected with wild-type HSV-1(F), and viral titers were assayed at various time points after infection. As shown in Fig. 8A, viral growth in HeLa/ΔSLC35E1/puro cells was lower than that in HeLa/puro or HeLa/ΔSLC35E1/SLC35E1 cells. The progeny virus titers in HeLa/ΔSLC35E1/puro cells at 36 h after

TABLE 2 Effect of the SLC35E1 KO on the distribution of virus particles in infected HeLa cells

Cell type	No. of intranuclear invaginations	% (no.) of virus particles in morphogenetic stage:					Total (no. of particles/no. of cells)
		Nucleocapsids in the nucleus	Enveloped virions in the perinuclear space	Nucleocapsids in the cytoplasm	Enveloped virions in the cytoplasm	Extracellular enveloped virions	
HeLa/puro	4	39.7 ± 4.2 (800)	4.0 ± 1.4 (83)	4.1 ± 0.7 (81)	9.9 ± 1.8 (211)	42.3 ± 4.7 (885)	2,060/10
HeLa/ΔSLC35E1/puro	20	33.7 ± 3.2 (800)	18.0 ± 3.4 (467)	4.4 ± 1.2 (97)	6.3 ± 1.1 (156)	37.7 ± 4.3 (903)	2,423/10
HeLa/ΔSLC35E1/SLC35E1	5	39.3 ± 5.5 (838)	3.9 ± 1.5 (89)	4.2 ± 1.5 (85)	8.7 ± 2.3 (187)	43.8 ± 4.6 (870)	2,069/10

infection were significantly lower than those in HeLa/puro or HeLa/ΔSLC35E1/SLC35E1 cells (Fig. 8B). These results indicated that SLC35E1 was required for efficient HSV-1 replication in cell cultures.

Effect of a mutation in the putative substrate binding site of SLC35E1 on HSV-1 nuclear egress and replication. The human SLC35 family is comprised of 31 hydrophobic and homologous proteins that are divided into 7 subfamilies, from SLC35A to SLC35G (49). Among these SLC35 family members, about one-third have been studied in detail. These were characterized as nucleotide sugar transporters (NSTs), which transport nucleotide sugar and adenosine 3′-phospho 5′-phosphosulfate from the cytosol to the endoplasmic reticulum (ER) and the Golgi apparatus, where they are required for the glycosylation and sulfation of proteins, lipids, and proteoglycans (49). In contrast, little is known about the remaining members of the SLC35 family, particularly the members of the SLC35E, SLC35F, and SLC35G subfamilies. Of note, a previous phylogenic analysis of over 250 NSTs from 20 species identified 10 clades. Of note, the clade to which SLC35E1 belongs contains the plastic phosphate translocator (pPT) family of proteins, which have various roles in the metabolic pathways of plants (50). A recent study (51, 52) identified 4 amino acid residues (Lys-204, Tyr-339, Lys-362, and Arg-363) in a pPT family protein, *Galdieria sulphuraria* glucose-6-phosphate/phosphate translocator (GsGPT), as the substrate binding sites, three of which (Lys-204, Lys-362, and Arg-363) are completely conserved in the clade members, including SLC35E1 (Lys-142, Lys-298, and Arg-299) (Fig. 9).

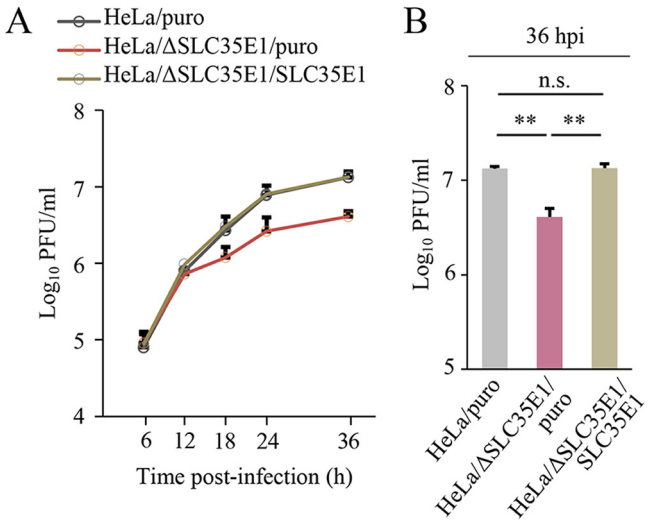

FIG 8 Effect of SLC35E1 KO on HSV-1 replication. (A) HeLa/puro, HeLa/ΔSLC35E1/puro, and HeLa/ΔSLC35E1/SLC35E1 cells were infected with wild-type HSV-1(F) at an MOI of 5. Total virus from the cell culture supernatants and infected cells was harvested and assayed on Vero cells. Each data point is the mean ± standard error of 3 independent experiments. (B) Progeny virus titers at 36 h postinfection. Data are shown as the mean ± standard error of three independent experiments. Statistical analysis was performed by one-way ANOVA and Tukey's test. **, $P < 0.01$; n.s., not significant.

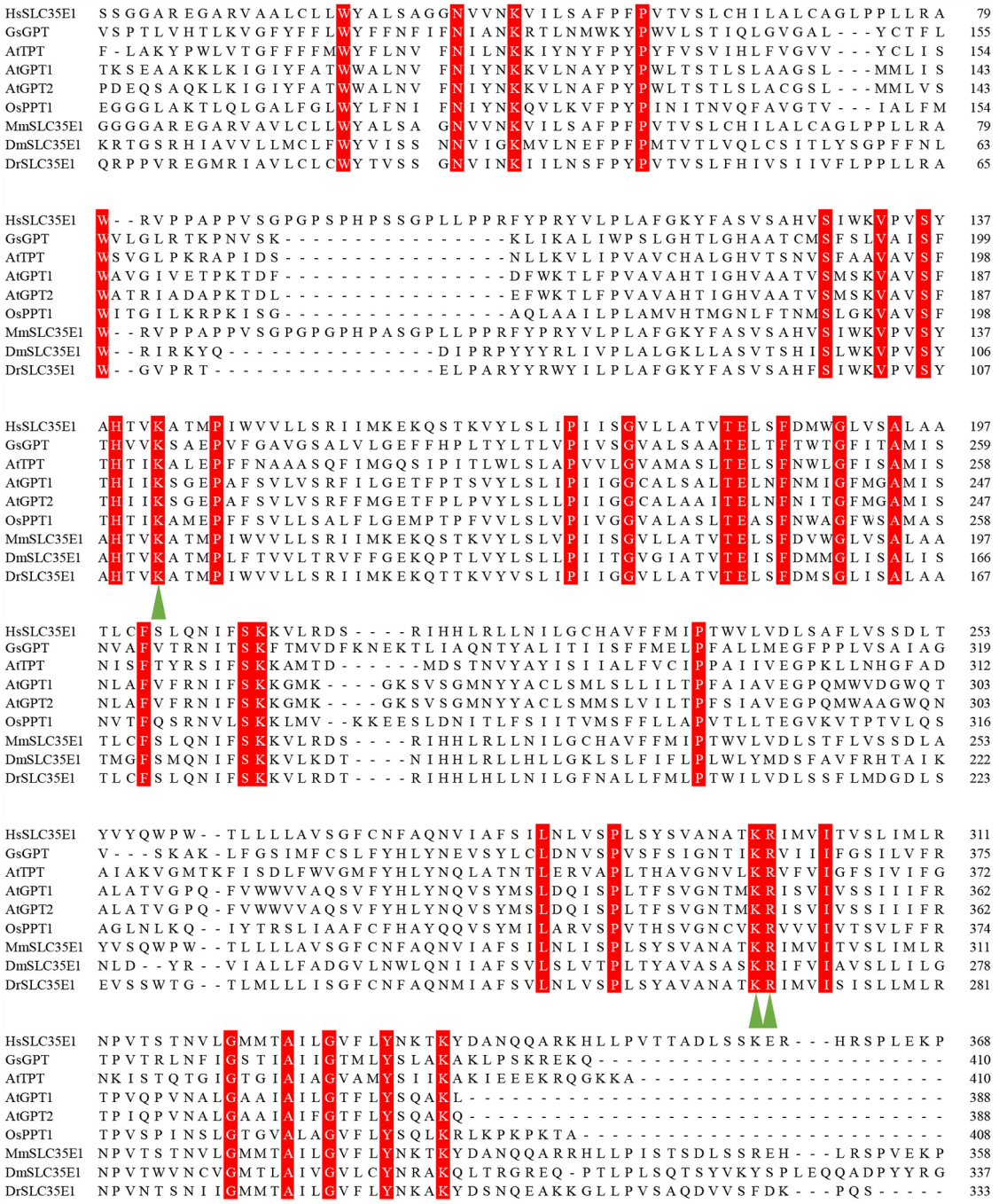

FIG 9 Amino acid sequence alignment of the SLC35E1 homologs. Alignment analysis was executed using the align tool of UniProt (https://www.uniprot.org/). Completely conserved amino acids among the homologs are highlighted in red. Green arrowheads indicate substrate binding amino acids of GsGPT.

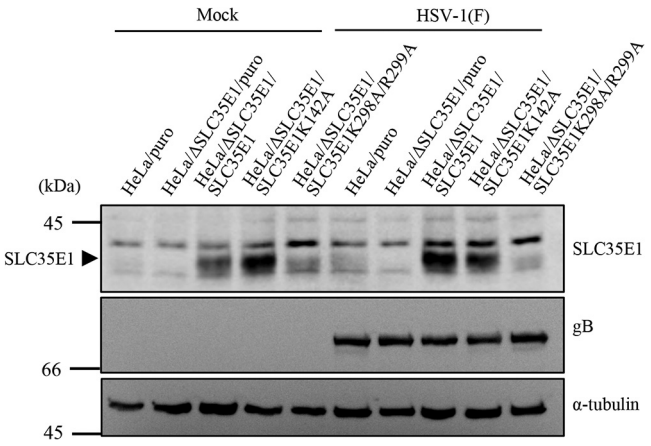

FIG 10 Effects of the K142A or the K298A/R299A mutation(s) in SLC35E1 on the accumulation of SLC35E1 in mock- or HSV-1-infected HeLa cells. HeLa/puro, HeLa/ΔSLC35E1/puro, HeLa/ΔSLC35E1/SLC35E1, HeLa/ΔSLC35E1/SLC35E1K142A, and HeLa/ΔSLC35E1/SLC35E1K298A/R299A cells were mock infected or infected with wild-type HSV-1(F) at an MOI of 5 for 22 h and analyzed by immunoblot with the indicated antibodies.

To investigate the effects of these conserved amino acid residues in SLC35E1 (Lys-142, Lys-298, and Arg-299) in HSV-1 nuclear egress, we generated HeLa/ΔSLC35E1 cells expressing either of the two SLC35E1 mutants with an alanine substitution(s) at Lys-142 or at Lys-298 and Arg-299 (HeLa/ΔSLC35E1/SLC35E1K142A or HeLa/ΔSLC35E1/SLC35E1K298A/R299A, respectively). As shown in Fig. 10, mock-infected HeLa/ΔSLC35E1/SLC35E1K298A/R299A cells, but not mock-infected HeLa/ΔSLC35E1/SLC35E1K142A cells, produced less SLC35E1 proteins than mock-infected HeLa/ΔSLC35E1/SLC35E1 cells. HSV-1(F)-infected HeLa/ΔSLC35E1/SLC35E1K298A/R299A cells produced much lower levels of SLC35E1 proteins than HSV-1(F)-infected HeLa/ΔSLC35E1/SLC35E1 cells, whereas HSV-1(F)-infected HeLa/ΔSLC35E1/SLC35E1K142A cells produced comparable levels of SLC35E1 proteins to HSV-1(F)-infected HeLa/ΔSLC35E1/SLC35E1 cells (Fig. 10). These results suggested that the K298A/R299A mutations in SLC35E1 reduced the accumulation of proteins in normal and HSV-1-infected cells. Therefore, we focused on the K142A mutation in SLC35E1 for further analyses.

To examine the effect of the K142A mutation in SLC35E1 on the redistribution of protein in HSV-1-infected cells, we generated HeLa cells expressing enhanced green fluorescent protein (EGFP)-SLC35E1 (HeLa/EGFP-SLC35E1) or EGFP-SLC35E1K142A (HeLa/EGFP-SLC35E1K142A). HeLa/EGFP-SLC35E1 or HeLa/EGFP-SLC35E1K142A cells were mock infected or infected with wild-type HSV-1(F) for 22 h and analyzed by confocal microscopy. As shown in Fig. 11, localization of EGFP-SLC35E1K142A was similar to that of EGFP-SLC35E1 in mock- or HSV-1-infected cells, suggesting that the K142A mutation in SLC35E1 had no obvious effect on the distribution of this protein in the absence or presence of HSV-1 infection.

HeLa/puro, HeLa/ΔSLC35E1/puro, HeLa/ΔSLC35E1/SLC35E1, and HeLa/ΔSLC35E1/SLC35E1K142A cells were infected with wild-type HSV-1(F) for 22 h, and the localization of UL34 and virion morphogenesis in these infected cells were analyzed by confocal and electron microscopy, respectively. The results (Fig. 12 and Table 3) were as follows. (i) Infected HeLa/ΔSLC35E1/SLC35E1K142A cells contained aberrant punctate structures of UL34 around the nuclear rim and in the nucleus at a level similar to that induced in infected HeLa/ΔSLC35E1/puro cells (Fig. 12A and B). (ii) In infected HeLa/ΔSLC35E1/SLC35E1K142A cells, membranous invagination structures containing PEVs were significantly induced adjacent to the NM, and PEVs were aberrantly accumulated in the perinuclear space and the invagination structures at levels similar to those observed in HeLa/ΔSLC35E1/puro cells (Fig. 12C and D and Table 3). Thus, the K142A mutation in SLC35E1 induced phenotypes that were almost identical to SLC35E1 KO.

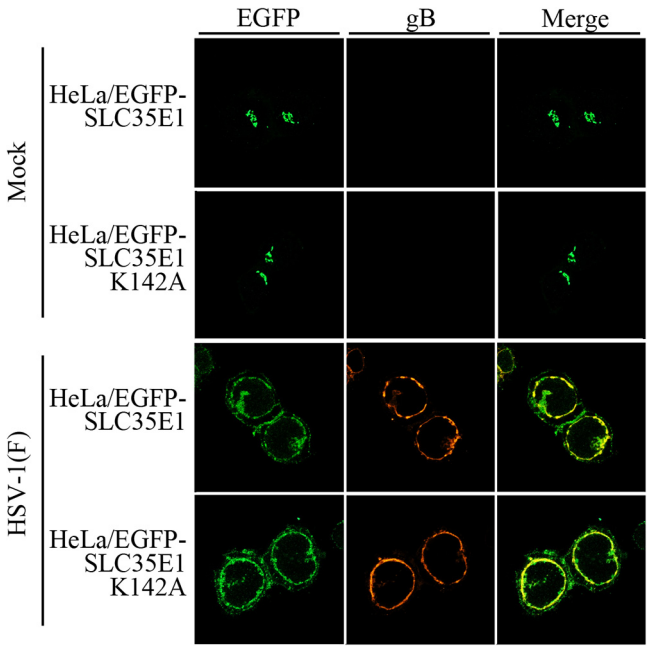

FIG 11 Effects of the K142A mutation in EGFP-SLC35E1 on the localization of EGFP-SLC35E1 in HeLa cells. HeLa/EGFP-SLC35E1 and HeLa/EGFP-SLC35E1K142A cells were mock infected or infected with wild-type HSV-1(F) at an MOI of 5 for 22 h, stained with anti-gB antibody, and examined by confocal microscopy.

These results suggested that the effect of SLC35E1 on HSV-1 nuclear egress was dependent on its function(s), which is impaired by the K142A mutation in the protein.

DISCUSSION

The induction of membranous invagination structures containing PEVs adjacent to the NM, as well as the accumulation of PEVs in the perinuclear space and invagination structures, is a characteristic phenotype of a mutation(s) or depletion of viral and cellular effectors in HSV-1 nuclear egress (31–37). This phenotype is commonly accompanied by another phenotype, the mislocalization of the NEC to punctate structures around the NM and in the nucleus (33, 34, 36, 37, 46). These phenotypes were previously reported for mutations that blocked the expression of Us3, its kinase activity, CD98hc, β1-integrin, p32 (31–34, 36, 37, 46, 53), the expression of gB and gH (35), the Us3 phosphorylation of gB and expression of gH (32), and the Us3 phosphorylation of UL31 (36). These phenotypes are thought to reflect an imbalance between the rate of virion delivery into the perinuclear space (primary envelopment) and the rate of egress from this space (de-envelopment): the rate of virion egress from the perinuclear space may be decreased, whereas the rate of egress may not change or not decrease as much. Therefore, the viral and cellular proteins listed above are thought to act in HSV-1 de-envelopment during viral nuclear egress.

In this study, we established a screening system to identify cellular effectors involved in HSV-1 nuclear egress by the interactome for HSV-1 NEC in combination with CRISPR/Cas9-based functional screening to target the cellular proteins identified in the interactome to detect the mislocalization of emerin caused by a defect in this viral procedure. This screening system identified SLC35E1, an orphan transporter, as a novel effector for HSV-1 nuclear egress, whose depletion exhibited phenotypes almost identical to those caused by the mutation or depletion of CD98hc, β1-integrin, p32, and Us3, gB, and gH, viral and cellular effectors involved in HSV-1 de-envelopment (31–37, 46), suggesting SLC35E1 acts in HSV-1 de-envelopment. Of note, HSV-1 de-envelopment and viral replication are not entirely dependent on any of these viral and cellular effectors, as observed here and in previous studies (31–36), although de-

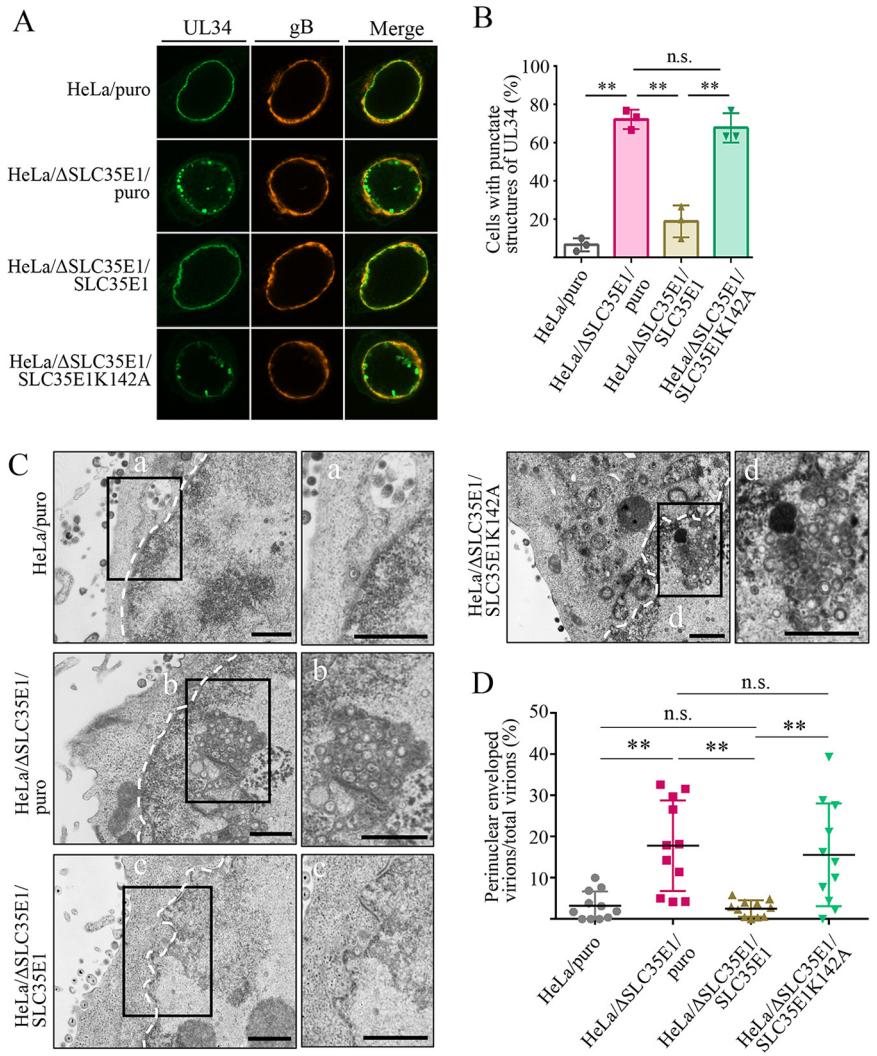

FIG 12 Effects of the K142A mutation in SLC35E1 on HSV-1 nuclear egress. (A) HeLa/puro, HeLa/ΔSLC35E1/puro, HeLa/ΔSLC35E1/SLC35E1, and HeLa/ΔSLC35E1/SLC35E1K142A cells were infected with wild-type HSV-1(F) at an MOI of 5 for 22 h, stained with anti-UL34 and anti-gB antibodies, and examined by confocal microscopy. (B) Percentage of cells with aberrant punctate structures at the nuclear rim and in the nucleus was determined. Data are shown as the mean ± standard error of 3 independent experiments. Statistical analysis was performed by one-way ANOVA with Turkey's test. **, $P < 0.01$; n.s., not significant. (C) HeLa/puro, HeLa/ΔSLC35E1/puro, HeLa/ΔSLC35E1/SLC35E1, and HeLa/ΔSLC35E1/SLC35E1K142A cells were infected with wild-type HSV-1(F) at an MOI of 20, fixed at 22 h postinfection, embedded, sectioned, stained, and examined by transmission electron microscopy. The images labeled a to d on the right are magnifications of the corresponding boxed areas on the left. Bars, 1 μm. Dotted lines indicate the nuclear membrane. (D) Mean proportions of enveloped virions in the perinuclear space of 10 infected cells were determined. Statistical analysis was performed by one-way ANOVA with Turkey's test. **, $P < 0.01$; n.s., not significant.

envelopment is considered a critical step in HSV-1 replication (3–6). Therefore, these viral and cellular proteins might have redundant functions in HSV-1 de-envelopment. In support of this, previous studies reported the redundancy of gB and gH, and Us3-mediated gB phosphorylation and gH, in HSV-1 de-envelopment (32, 35). Alternatively, unknown critical factor(s) for HSV-1 de-envelopment might be involved. Furthermore, we should note that the number, size, and distribution of the punctate structures of the NEC induced by depletion of each of the HSV-1 and cellular de-envelopment factors shown in this and earlier studies varied (31–36). Therefore, we cannot eliminate the possibility that these factors act differently in HSV-1 de-envelopment.

At present, the mechanism by which SLC35E1 promotes HSV-1 de-envelopment

TABLE 3 Effect of the K142A mutation in SLC35E1 on the distribution of virus particles in infected HeLa cells

Cell type	No. of intranuclear invaginations	% (no.) of virus particles in morphogenetic stage:					Total (no. of particles/no. of cells)
		Nucleocapsids in the nucleus	Enveloped virions in the perinuclear space	Nucleocapsids in the cytoplasm	Enveloped virions in the cytoplasm	Extracellular enveloped virions	
HeLa/puro	1	36.4 ± 4.6 (724)	3.3 ± 1.2 (60)	5.1 ± 1.3 (91)	8.4 ± 2.3 (155)	46.9 ± 4.7 (884)	1,914/10
HeLa/ΔSLC35E1/puro	21	30.4 ± 3.9 (720)	17.8 ± 3.7 (393)	3.8 ± 1.3 (68)	4.1 ± 1.5 (81)	44.0 ± 3.4 (904)	2,166/10
HeLa/ΔSLC35E1/SLC35E1	4	37.4 ± 3.7 (746)	2.5 ± 0.7 (55)	4.6 ± 1.8 (93)	7.1 ± 1.7 (148)	48.3 ± 4.0 (941)	1,983/10
HeLa/ΔSLC35E1/SLC35E1K142A	18	32.6 ± 3.8 (764)	15.5 ± 4.2 (355)	3.9 ± 1.1 (82)	4.3 ± 1.0 (82)	43.8 ± 4.9 (903)	2,186/10

remains unclear. One possibility is that SLC35E1 on the ONM interacts with a molecule (s) on PEVs to promote de-envelopment fusion between the PEV envelopes and the ONM. The human SLC superfamily, the largest superfamily of membrane transport proteins, has over 400 annotated members and accounts for approximately 20% of all membrane proteins encoded by the human genome (54–56). Of note, at least 10 proteins in the SLC superfamily function as entry receptors for retroviruses (57). Furthermore, CD98hc, previously identified as a cellular effector of HSV-1 de-envelopment (33), also belongs to the SLC superfamily (called SLC3A2). Interestingly, CD98hc promoted the cellular entry of hepatitis C virus (58) and regulated membrane fusion mediated by fusogenic viral envelope glycoproteins and/or their cofactors, including the F and HN proteins of Newcastle disease virus and human parainfluenza virus type 2 and gp120 of human immunodeficiency virus (59–62). Although the target membranes differ for de-envelopment and viral entry, the de-envelopment fusion of herpesviruses uses a mechanism similar to membrane fusion during the viral entry of these envelope viruses. Therefore, a common mechanism might be involved for the membrane fusion between cellular membranes and viral envelopes mediated by these SLC family members, including SLC35E1.

In this study, we showed that during HSV-1 de-envelopment, SLC35E1 required a conserved amino acid residue, which corresponded to one of the essential substrate binding sites in the well-characterized transporter GsGPT (52). These observations raised another possibility that the transporter activity of SLC35E1 contributes to HSV-1 de-envelopment fusion. Although membrane fusion is usually induced by large molecules such as proteins and peptides (63), accumulating evidence suggests that small molecules and ions can also mediate or promote membrane fusion (64). The SLC superfamily proteins transport a wide variety of molecules, including sugars, amino acids, vitamins, nucleotides, metals, inorganic ions, organic anions, oligopeptides, and drugs (54–56, 65). Furthermore, SLC proteins belonging to structurally dissimilar families or folds have chemically similar substrates, whereas, in contrast, those belonging to the same fold or family do not always share substrate specificity (66). Therefore, although the substrate(s) of SLC35E1 remain to be identified, its (their) dynamics in the perinuclear space might be involved in HSV-1 de-envelopment fusion. Further studies to identify and characterize substrate(s) of SLC35E1 on the NM during HSV-1 infection, as well as that of the substrates of another SLC family member, CD98hc, in HSV-1 de-envelopment fusion are of interest and are underway in our laboratory. Of note, mutations in two highly conserved amino acid residues in SLC20A2, an entry receptor for murine, gibbon ape, and feline leukemia viruses on the plasma membrane or endosome membrane (57), abolished transporter activity but had little effect on its viral receptor function (67). These observations suggest the viral receptor function of SLC20A2 is independent of its transporter function (67). Which SLC protein substrates are involved in membrane fusion might depend on the target membranes and factors involved. However, there is the possibility that defects in HSV-1 nuclear egress observed with the SLC35E1K142A mutant were associated with the steric hindrance and alternation of stability, folding, and other function(s) of SLC35E1 caused by the K142A mutation rather than inhibition of the transport activity of SLC35E1.

Although some of the mechanisms involved during herpesvirus primary envelopment have gradually been elucidated (3, 6), very little is known about the mechanisms of de-envelopment and the other steps involved in primary envelopment. To understand the whole picture of herpesvirus nuclear egress, future studies should identify additional cellular effectors involved in these procedures. To date, various viral and cellular effectors, other than the NEC, have been reported in herpesvirus nuclear egress; therefore, the new screening system established in this study using known effectors as bait might be useful for those studies.

MATERIALS AND METHODS

Cells and viruses. Vero, HeLa, HaCaT, rabbit skin, HEK293FT, and Plat-GP cells were described previously (37, 47, 68–70). HSV-1 wild-type strain HSV-1(F) and recombinant virus YK511 (Us3K220M) encoding an enzymatically inactive Us3 mutant in which lysine at UL3 residue 220 was replaced with methionine were described previously (48).

Plasmids. pBS-SEM-KanS was constructed by cloning a kanamycin resistance cassette and the I-SceI recognition site, amplified by PCR from pEPkan-S (71) using primers that additionally encode the tandem strep epitopes-TEV protease cleavage site, 5′-GCGAATTCATGGCTAGCTGGAGCCACCCGCAGTTCGAGAAAGGTGGAGGTGCCCGAGGTGGATCGGGAGGTGGATCGTGGAGCCACCCGCAGTTCGAAAAAGGAGGAGGATGACGACGATAAGTAGGG-3′ and 5′-GCGTCGACCAAGTCCTCTTCAGAAATGAGCTTTTGCTCACCCTGAAAATACAAATTCTCTGAACCTCCTTTTTCGAACTGCGGGTGGCTCCACGATCCACCTCCAACCAATTAACCAATTCTGATTAG-3′ into pBluescript II KS(+) (Stratagene). pRetroX-TRE3G-hSpCas9 was constructed by cloning the hSpCas9 open reading frame (ORF), amplified by PCR from pX459V2.0 (Addgene), into pRetroX-TRE3G (Clontech). pVenusA206K-N1 was constructed by cloning the VenusA206K ORF, amplified by PCR from pBS-VenusA206K (47), into the BamHI-NotI site of pEGFP-N1 (Clontech). Pemerin-VenusA206K encoding emerin fused to VenusA206K at the carboxyl terminus was constructed by cloning the emerin ORF, amplified by PCR from cDNAs synthesized from the total RNAs of HeLa cells, into pVenusA206K-N1 in frame with VenusA206K. Emerin-VenusA206K ORF, amplified by PCR from pemerin-VenusA206K, was cloned into pMXs-puro (68) to yield pMXs-emerin-VenusA206K-puro. pcDNA3.1(+)-SLC35E1 was constructed by cloning the SLC35E1 ORF, amplified by PCR from cDNAs synthesized from the total RNAs of HeLa cells, into pcDNA3.1(+) (Invitrogen). A DNA fragment of pcDNA3.1(+)-SLC35E1 encoding SLC35E1 was cloned into pMXs-puro to yield pMXs-SLC35E1-puro. pcDNA3.1(+)-SLC35E1K142A and pcDNA3.1(+)-SLC35E1K298A/R299A encoding SLC35E1 carrying the K142A or the K298A/R299A mutation, respectively, were generated by the fusion PCR method. The primers used for pcDNA3.1(+)-SLC35E1K142A were 5′-ACACACCGTCGCAGCCACCATGC-3′ and 5′-GCCTCGAGTTACACATCATAGCGGTTCAAAC-3′ and 5′-GCATGGTGGCTGCGACGGTGTGT-3′ and 5′-GCGAATTCATGGCGGCGGCCGCGGTGG-3′ in the 1st PCR and 5′-GCGAATTCATGGCGGCGGCCGCGGTGG-3′ and 5′-GCCTCGAGTTACACATCATAGCGGTTCAAAC-3′ in the 2nd PCR, and those used for pcDNA3.1(+)-SLC35E1K298/R299A were 5′-CAATGCCACCGCAGCCATCATGGTCA-3′ and 5′-GCCTCGAGTTACACATCATAGCGGTTCAAAC-3′ and 5′-TGACCATGATGGCTGCGGTGGCATTG-3′ and 5′-GCGAATTCATGGCGGCGGCCGCGGTGG-3′ in the 1st PCR, and 5′-GCGAATTCATGGCGGCGGCCGCGGTGG-3′ and 5′-GCCTCGAGTTACACATCATAGCGGTTCAAAC-3′ in the 2nd PCR. A DNA fragment of pcDNA3.1(+)-SLC35E1K142A encoding SLC35E1K142A was cloned into pMXs-puro to yield pMXs-SLC35E1K142A-puro. A DNA fragment of pcDNA3.1(+)-SLC35E1K298A/R299A encoding SLC35E1K298A/R299A was cloned into pMXs-puro to yield pMXs-SLC35E1K298A/R299A-puro. pEGFP-SLC35E1 encoding SLC35E1 fused to EGFP at the amino terminus was constructed by cloning the SLC35E1 ORF, amplified by PCR from pcDNA3.1(+)-SLC35E1, into pEGFP-C1 (Clontech) in frame with EGFP. EGFP-SLC35E1 ORF, amplified by PCR from pEGFP-SLC35E1, was cloned into pMXs-puro to yield pMXs-EGFP-SLC35E1-puro. pMXs-EGFP-SLC35E1K142A-puro encoding SLC35E1K142A fused to EGFP at the amino terminus was generated by the fusion PCR method described above. The primers used for pMXs-EGFP-SLC35E1K142A-puro were 5′-ACACCGTCGAGGCCACCATGCCCATCTGGGT-3′ and 5′-GCCTCGAGCTACACATCATAGCGGTTCA-3′ and 5′-ACCCAGATGGGCATGGTGGCCTCGACGGTGT-3′ and 5′-GCGGATCCATGGTGAGCAAGGGCGAGGA-3′ in the 1st PCR and 5′-GCGGATCCATGGTGAGCAAGGGCGAGGA-3′ and 5′-GCCTCGAGCTACACATCATAGCGGTTCA-3′ in the 2nd PCR. To construct pX459V2.0-SLC35E1, sense and antisense oligonucleotides were designed for insertion into the BbsI site in the pX459V2.0 bicistronic expression vector (Addgene), which expresses Cas9 and synthetic sgRNA as follows: 5′-CACCGGAGGACCACCCAGATGGGCA-3′ and 5′-AAACTGCCCATCTGGGTGGTCCTCC-3′. The DNA oligonucleotides were annealed and incorporated into a pX459V2.0 vector linearized with the BbsI restriction enzyme.

Mutagenesis of viral genomes and generation of recombinant HSV-1. Recombinant virus YK742 (SE-UL34/Flag-UL31) encoding UL34 fused to a tandem strep epitope-(TEV) protease cleavage site (SE-UL34) at the amino terminus and UL31 fused to Flag epitope tag (Flag-UL31), in which the tag was inserted at UL31 amino acid residue 49 (Fig. 1A), were generated by a two-step Red-mediated mutagenesis procedure as described previously (48) except for the use of *Escherichia coli* GS1783 containing pYEbac102, a full-length infectious HSV-1(F) clone (69), using the primers 5′-GAACCCTTTGGTGGGTTTACGCGGGCACGCACGCTCCCATCGCGGGCGCCATGGCTAGCTGGAGCCACCC-3′, 5′-TCGAAGGCGTCACCTGGGTGGCCGGTGTAGGGCTTGCCCAGTCCCGCCATACCCTGAAAATACAAATTCT-3′, 5′-GGTGCGTCGGGCCTCCCGGAAGAGCCTGCCGCCTCACGCCGACTACAAGGATGACGATGACAAGCGCAAACAAGGATGACGACGATAAGTAGGG-3′, 5′-GATAGCGCTGGCGCTCGTGTAAACACAGCTCCTGTTTGCGCTTGTCATCGTCATCCTTGTAGTCGGCGTGAGCAACCAATTAACCAATTCTGATTAG-3′, and pBS-SEM-KanS.

Antibodies. The commercial antibodies used in this study were mouse monoclonal antibodies to Flag (M2; Sigma), α-tubulin (clone DM1A; Sigma), emerin (clone 4G5; catalog no. MS-1751-S; Neomarkers), gB (catalog no. P1105; Virusys), Strep-tag (code M211-3; MBL), and Cas9 (7A9-3A3; CST), and rabbit polyclonal antibodies to GFP (code 598; MBL), SLC35E1 (catalog no. ab121501; Abcam), and lamin B1 (catalog no. ab16048-100; Abcam). Mouse polyclonal antibodies to UL31 and rabbit polyclonal antibodies to UL34 and UL50 were reported previously (22, 72).

Identification of proteins that interact with the UL34 and UL31 complex. HaCaT cells were infected with YK742 (SE-UL34/Flag-UL31) at a multiplicity of infection (MOI) of 3, harvested at 24 h postinfection, and lysed in NP-40 buffer (50 mM Tris-HCl [pH 8.0], 120 mM NaCl, 50 mM NaF, and 0.5% NP-40) containing a protease inhibitor cocktail (Nacalai Tesque). After centrifugation, the supernatants were reacted with Strep-Tactin Sepharose (IBA) with rotation for 2 h at 4°C. The precipitates were collected by brief centrifugation and washed extensively with NP-40 buffer, and the precipitates were incubated with AcTEV protease (Invitrogen) overnight at 4°C. After another centrifugation, the supernatants were immunoprecipitated with an anti-Flag M2 affinity gel (Sigma), and the immunoprecipitates were washed twice with NP-40 buffer. Flag elution buffer (50 mM Tris-HCl [pH 8.0], 150 mM NaCl, and 0.5 mg of Flag peptide/mL) was added, and the immunoprecipitates were rotated for 10 h at 4°C. The eluted proteins were digested into peptides using the filter-aided sample preparation (FASP) method (73). Briefly, the eluted protein solution was loaded onto a centrifugal filter (Amicon Ultra 0.5-mL centrifugal filter 30K; Merck Millipore), and the detergent was removed by washing 4 times with a filter buffer (50 mM Tris-HCl [pH 8.2], 0.15 M NaCl). The proteins were then reduced by incubation with 10 mM dithiothreitol for 90 min, alkylated with 55 mM iodoacetamide for 30 min, treated by buffer exchange with 50 mM ammonium bicarbonate, and digested with trypsin for 18 h at 37°C. The peptide solutions were acidified using 1% trifluoroacetic acid, desalted with ZipTip C_{18} resin (Merck Millipore), and evaporated to a maximum volume of 10 μL by a vacuum concentrator. Peptides were analyzed by a Dina-2A nanoflow liquid chromatography (LC) system (KYA Technologies) coupled with an LTQ Orbitrap Velos mass spectrometer (Thermo Fisher Scientific). Proteins were identified by analyzing the mass spectrometry (MS) and the MS/MS signals against the 68,711 protein sequences in the RefSeq human protein database (National Center for Biotechnology Information) and the 74 virus protein sequences based on the complete genome sequence of human herpesvirus 1 strain F (GenBank accession number GU734771) using the Mascot algorithm (v2.4.1; Matrix Science) with the following parameters: fixed modification, carbamidomethylation (Cys); variable modifications, oxidation (Met), protein N-terminal acetylation, pyroglutamination (Gln), phosphorylation (Ser, Thr, and Tyr), and diglycine-modified lysine (Lys); maximum missed cleavages, 2; peptide mass tolerance, 3 ppm; and MS/MS tolerance, 0.8 Da. For peptide identification, we conducted decoy database searching by Mascot and applied a filter to satisfy a false-positive rate lower than 1%.

Establishment of HeLa/tet-on Cas9/emerin-VenusA206K cells. HeLa cells were transduced simultaneously with supernatants from Plat-GP cells, a 293T-derived murine leukemia virus-based packaging cell line, cotransfected with pMDG (74) and pRetroX-TRE3G-hSpCas9 or supernatants from cells cotransfected with pMDG and pRetroX-Tet3G, and selected with 500 μg/mL G418 (Wako) and 1 μg/mL of puromycin (Sigma). The resultant cells were further transduced with supernatants from Plat-GP cells cotransfected with pMXs-emerin-VenusA206K-puro and pMDG, cloned from a single colony showing Venus fluorescence, and designated HeLa/tet-on Cas9/emerin-VenusA206K cells.

CRISPR/Cas9 screening using HeLa/tet-on Cas9/emerin-VenusA206K cells. Based on information from Addgene pool library no. 1000000067, including 178,896 sgRNAs against 18,166 human genes, template DNAs for sgRNAs (10 sgRNAs against each of the 738 cellular genes whose products were identified as putative NEC-interacting proteins by the interactome screening above) were synthesized by CustomArray, Inc., amplified by PCR using the primers 5′-ATCTTGTGGAAAGGACGAAACACC-3′ and 5′-ACTTGCTATTTCTAGCTCTTAAAC-3′, and cloned into a lentivirus vector pKLV2-U6gRNA5(BbsI)-PGKpuro2ABFP-W using the NEBuilder HiFi DNA assembly cloning kit (New England Biolabs) (Fig. 3A). HeLa/tet-on Cas9/emerin-VenusA206K cells were transduced with supernatants from HEK293FT cells transfected with the resultant lentivirus vector library using the ViraPower lentiviral expression system (Invitrogen) (Fig. 3A). In these cells, the frequency of blue fluorescence protein (BFP)-positive cells, including the guide RNA (gRNA) library with the BFP sequence, was approximately 20%. VenusA206K and BFP double-positive cell populations were sorted by FACSAria II (BD Life Sciences) and left for 2 weeks in the presence of 1 μg/mL of doxycycline to generate a mutant cell pool (Fig. 3A). Then, 100 cells from the mutant cell pool per well were seeded onto 96-well plates, incubated, and split into 2 identical 96-well plates (Fig. 3B). Cells on one plate were infected with 3×10^5 PFU of wild-type HSV-1 (F) for 22 h and analyzed to detect aberrant punctate structures of emerin-VenusA206K adjacent to the NM by fluorescence microscopy (Fig. 3B). When punctate structures of emerin-VenusA206K were detected, cells on the corresponding well in the plate were seeded onto new 96-well plates (20 cells per well), incubated, split into two identical 96-well plates, and analyzed as described above (Fig. 3B). These processes were repeated until cell clones showing the punctate structures of emerin-VenusA206K in the presence of HSV-1 infection were isolated (Fig. 3B). Finally, sgRNA sequences from the positive cell clones were determined (Fig. 3B). sgRNA sequences were amplified by PCR and sequenced directly using the primers 5′-GCTCTAGACCCTACGCGTTACTCGAGCCAAG-3′ and/or 5′-GCGAATTCGTGGATGTGGAATGTGTGCG-3′.

Establishment of HeLa/SLC35E1, HeLa/EGFP-SLC35E1, and HeLa/EGFP-SLC35E1K142A cells. HeLa cells were transduced with supernatants from Plat-GP cells cotransfected with pMDG in combination with pMXs-SLC35E1-puro, pMXs-EGFP-SLC35E1-puro, or pMXs-EGFP-SLC35E1K142A-puro, selected with 1 μg/mL of puromycin, and designated HeLa/EGFP-SLC35E1 and HeLa/EGFP-SLC35E1K142A cells, respectively.

Establishment of HeLa/ΔSLC35E1 cells and their derivatives. HeLa cells were transfected with pX459V2.0-SLC35E1 using a NEPA21 electroporator (Nepa Gene), selected with 1 μg/mL puromycin for 48 h, cloned from a single colony, and designated HeLa/ΔSLC35E1 cells. To determine the genotypes of each allele from HeLa/ΔSLC35E1 cells, genomic DNA from these cells was amplified by PCR and sequenced directly. The sequencing of PCR products showed mixed patterns of sequences, and therefore, PCR products were cloned into plasmids, and their sequences were determined. We obtained four patterns of sequences, which represented the SLC35E1 sequences of the 4 SLC35E1 alleles from HeLa/ΔSLC35E1 cells and did not include a pattern of the wild-type sequence. For controls, HeLa cells were transduced with supernatants from Plat-GP cells cotransfected with pMDG and pMXs-puro, selected with 1 μg/mL puromycin, and designated HeLa/puro cells.

HeLa/ΔSLC35E1 cells were further transduced with supernatants from Plat-GP cells cotransfected with pMDG in combination with pMXs-puro, pMXs-SLC35E1, pMXs-SLC35E1K142A, and pMXs-SLC35E1K298A/R299A, selected with 1 μg/mL puromycin, and designated HeLa/ΔSLC35E1/puro, HeLa/ΔSLC35E1/SLC35E1, HeLa/ΔSLC35E1/SLC35E1K142A, and HeLa/ΔSLC35E1/SLC35E1K298A/R299A cells, respectively.

Immunoblotting, immunoprecipitation, and immunofluorescence. Immunoblotting and immunofluorescence were performed as described previously (33, 75, 76).

Electron microscopy. HeLa cells or their derivatives were infected with wild-type HSV-1(F) at an MOI of 20 for 22 h. The infected cells were fixed with 2% paraformaldehyde and 2% glutaraldehyde overnight at 4°C, postfixed with 2% osmium tetroxide on ice for 2 h, washed with distilled water, dehydrated with an ethanol gradient series, incubated in propylene oxide, and embedded in an Epon 812 resin mixture. Then, the samples were sectioned on grids, stained with 2% uranyl acetate and Reynold's lead citrate, and examined by transmission electron microscopy (TEM) (77).

Assay for cell viability. The viability of HeLa/puro, HeLa/ΔSLC35E1/puro, and HeLa/ΔSLC35E1/SLC35E1 cells was assayed using Cell Counting Kit-8 (Dojindo) according to the manufacturer's instructions.

Statistical analysis. For the comparison of two groups, statistical analysis was performed using the unpaired Student's *t* test. Tukey's test was used for multiple comparisons. A *P* value of >0.05 was considered not significant (NS). All statistical analyses were performed using GraphPad Prism 7 (GraphPad Software, San Diego, CA). No methods were used to determine whether the data met the assumptions of the statistical approach.

ACKNOWLEDGMENTS

We thank Hiroshi Sagara, Toru Ikegami, Risa Abe, and Keiko Sato for their excellent technical assistance.

This study was supported by Grants for Scientific Research and Grant-in-Aid for Scientific Research (S) (20H05692) from the Japan Society for the Promotion of Science (JSPS); grants for Scientific Research on Innovative Areas from the Ministry of Education, Culture, Science, Sports and Technology of Japan (16H06433, 16H06429, 16K21723, 20H04899, 21H00338, and 21H00417); the Research Program on Emerging and Re-emerging Infectious Diseases (19fk018105h, 20wm0125002h, 20wm0225017s, 20wm0225009h, and 20wm0225003s) from the Japan Agency for Medical Research and Development (AMED); a grant from the International Joint Research Project of the Institute of Medical Science, the University of Tokyo; and grants from the Takeda Science Foundation and the Mitsubishi Foundation.

REFERENCES

1. Baines JD. 2011. Herpes simplex virus capsid assembly and DNA packaging: a present and future antiviral drug target. Trends Microbiol 19:606–613. https://doi.org/10.1016/j.tim.2011.09.001.
2. Cardone G, Heymann JB, Cheng N, Trus BL, Steven AC. 2012. Procapsid assembly, maturation, nuclear exit: dynamic steps in the production of infectious herpesvirions. Adv Exp Med Biol 726:423–439. https://doi.org/10.1007/978-1-4614-0980-9_19.
3. Draganova EB, Thorsen MK, Heldwein EE. 2021. Nuclear egress. Curr Issues Mol Biol 41:125–170. https://doi.org/10.21775/cimb.041.125.
4. Johnson DC, Baines JD. 2011. Herpesviruses remodel host membranes for virus egress. Nat Rev Microbiol 9:382–394. https://doi.org/10.1038/nrmicro2559.
5. Mettenleiter TC, Müller F, Granzow H, Klupp BG. 2013. The way out: what we know and do not know about herpesvirus nuclear egress. Cell Microbiol 15:170–178. https://doi.org/10.1111/cmi.12044.
6. Arii J. 2021. Host and viral factors involved in nuclear egress of herpes simplex virus 1. Viruses 13:754. https://doi.org/10.3390/v13050754.
7. Bigalke JM, Heuser T, Nicastro D, Heldwein EE. 2014. Membrane deformation and scission by the HSV-1 nuclear egress complex. Nat Commun 5:4131. https://doi.org/10.1038/ncomms5131.
8. Bigalke JM, Heldwein EE. 2015. Structural basis of membrane budding by the nuclear egress complex of herpesviruses. EMBO J 34:2921–2936. https://doi.org/10.15252/embj.201592359.
9. Klupp BG, Granzow H, Fuchs W, Keil GM, Finke S, Mettenleiter TC. 2007. Vesicle formation from the nuclear membrane is induced by coexpression of two conserved herpesvirus proteins. Proc Natl Acad Sci U S A 104:7241–7246. https://doi.org/10.1073/pnas.0701757104.
10. Hagen C, Dent KC, Zeev-Ben-Mordehai T, Grange M, Bosse JB, Whittle C, Klupp BG, Siebert CA, Vasishtan D, Bauerlein FJ, Cheleski J, Werner S, Guttmann P, Rehbein S, Henzler K, Demmerle J, Adler B, Koszinowski U, Schermelleh L, Schneider G, Enquist LW, Plitzko JM, Mettenleiter TC, Grunewald K. 2015. Structural basis of vesicle formation at the inner nuclear membrane. Cell 163:1692–1701. https://doi.org/10.1016/j.cell.2015.11.029.
11. Zeev-Ben-Mordehai T, Weberruß M, Lorenz M, Cheleski J, Hellberg T, Whittle C, El Omari K, Vasishtan D, Dent KC, Harlos K, Franzke K, Hagen C, Klupp BG, Antonin W, Mettenleiter TC, Grünewald K. 2015. Crystal structure of the herpesvirus nuclear egress complex provides insights into inner nuclear membrane remodeling. Cell Rep 13:2645–2652. https://doi.org/10.1016/j.celrep.2015.11.008.
12. Hetzer MW. 2010. The nuclear envelope. Cold Spring Harb Perspect Biol 2:a000539. https://doi.org/10.1101/cshperspect.a000539.
13. Bjerke SL, Roller RJ. 2006. Roles for herpes simplex virus type 1 UL34 and US3 proteins in disrupting the nuclear lamina during herpes simplex virus

type 1 egress. Virology 347:261–276. https://doi.org/10.1016/j.virol.2005.11.053.
14. Mou F, Forest T, Baines JD. 2007. US3 of herpes simplex virus type 1 encodes a promiscuous protein kinase that phosphorylates and alters localization of lamin A/C in infected cells. J Virol 81:6459–6470. https://doi.org/10.1128/JVI.00380-07.
15. Mou F, Wills EG, Park R, Baines JD. 2008. Effects of lamin A/C, lamin B1, and viral US3 kinase activity on viral infectivity, virion egress, and the targeting of herpes simplex virus U(L)34-encoded protein to the inner nuclear membrane. J Virol 82:8094–8104. https://doi.org/10.1128/JVI.00874-08.
16. Leach N, Bjerke SL, Christensen DK, Bouchard JM, Mou F, Park R, Baines J, Haraguchi T, Roller RJ. 2007. Emerin is hyperphosphorylated and redistributed in herpes simplex virus type 1-infected cells in a manner dependent on both UL34 and US3. J Virol 81:10792–10803. https://doi.org/10.1128/JVI.00196-07.
17. Morris JB, Hofemeister H, O'Hare P. 2007. Herpes simplex virus infection induces phosphorylation and delocalization of emerin, a key inner nuclear membrane protein. J Virol 81:4429–4437. https://doi.org/10.1128/JVI.02354-06.
18. Wang Y, Yang Y, Wu S, Pan S, Zhou C, Ma Y, Ru Y, Dong S, He B, Zhang C, Cao Y. 2014. p32 is a novel target for viral protein ICP34.5 of herpes simplex virus type 1 and facilitates viral nuclear egress. J Biol Chem 289:35795–35805. https://doi.org/10.1074/jbc.M114.603845.
19. Wu S, Pan S, Zhang L, Baines J, Roller R, Ames J, Yang M, Wang J, Chen D, Liu Y, Zhang C, Cao Y, He B. 2016. Herpes simplex virus 1 induces phosphorylation and reorganization of lamin A/C through the γ134.5 protein that facilitates nuclear egress. J Virol 90:10414–10422. https://doi.org/10.1128/JVI.01392-16.
20. Muranyi W, Haas J, Wagner M, Krohne G, Koszinowski UH. 2002. Cytomegalovirus recruitment of cellular kinases to dissolve the nuclear lamina. Science 297:854–857. https://doi.org/10.1126/science.1071506.
21. Park R, Baines JD. 2006. Herpes simplex virus type 1 infection induces activation and recruitment of protein kinase C to the nuclear membrane and increased phosphorylation of lamin B. J Virol 80:494–504. https://doi.org/10.1128/JVI.80.1.494-504.2006.
22. Liu Z, Kato A, Shindo K, Noda T, Sagara H, Kawaoka Y, Arii J, Kawaguchi Y. 2014. Herpes simplex virus 1 UL47 interacts with viral nuclear egress factors UL31, UL34, and Us3 and regulates viral nuclear egress. J Virol 88:4657–4667. https://doi.org/10.1128/JVI.00137-14.
23. Maruzuru Y, Shindo K, Liu Z, Oyama M, Kozuka-Hata H, Arii J, Kato A, Kawaguchi Y. 2014. Role of herpes simplex virus 1 immediate early protein ICP22 in viral nuclear egress. J Virol 88:7445–7454. https://doi.org/10.1128/JVI.01057-14.
24. Lv Y, Zhou S, Gao S, Deng H. 2019. Remodeling of host membranes during herpesvirus assembly and egress. Protein Cell 10:315–326. https://doi.org/10.1007/s13238-018-0577-9.
25. Leach NR, Roller RJ. 2010. Significance of host cell kinases in herpes simplex virus type 1 egress and lamin-associated protein disassembly from the nuclear lamina. Virology 406:127–137. https://doi.org/10.1016/j.virol.2010.07.002.
26. Reynolds AE, Liang L, Baines JD. 2004. Conformational changes in the nuclear lamina induced by herpes simplex virus type 1 require genes U(L)31 and U(L)34. J Virol 78:5564–5575. https://doi.org/10.1128/JVI.78.11.5564-5575.2004.
27. Takeshima K, Arii J, Maruzuru Y, Koyanagi N, Kato A, Kawaguchi Y. 2019. Identification of the capsid binding site in the herpes simplex virus 1 nuclear egress complex and its role in viral primary envelopment and replication. J Virol 93:e01290-19. https://doi.org/10.1128/JVI.01290-19.
28. Yang K, Baines JD. 2011. Selection of HSV capsids for envelopment involves interaction between capsid surface components pUL31, pUL17, and pUL25. Proc Natl Acad Sci U S A 108:14276–14281. https://doi.org/10.1073/pnas.1108564108.
29. Yang K, Wills E, Lim HY, Zhou ZH, Baines JD. 2014. Association of herpes simplex virus pUL31 with capsid vertices and components of the capsid vertex-specific complex. J Virol 88:3815–3825. https://doi.org/10.1128/JVI.03175-13.
30. Arii J, Watanabe M, Maeda F, Tokai-Nishizumi N, Chihara T, Miura M, Maruzuru Y, Koyanagi N, Kato A, Kawaguchi Y. 2018. ESCRT-III mediates budding across the inner nuclear membrane and regulates its integrity. Nat Commun 9:3379. https://doi.org/10.1038/s41467-018-05889-9.
31. Reynolds AE, Wills EG, Roller RJ, Ryckman BJ, Baines JD. 2002. Ultrastructural localization of the herpes simplex virus type 1 UL31, UL34, and US3 proteins suggests specific roles in primary envelopment and egress of nucleocapsids. J Virol 76:8939–8952. https://doi.org/10.1128/jvi.76.17.8939-8952.2002.
32. Wisner TW, Wright CC, Kato A, Kawaguchi Y, Mou F, Baines JD, Roller RJ, Johnson DC. 2009. Herpesvirus gB-induced fusion between the virion envelope and outer nuclear membrane during virus egress is regulated by the viral US3 kinase. J Virol 83:3115–3126. https://doi.org/10.1128/JVI.01462-08.
33. Hirohata Y, Arii J, Liu Z, Shindo K, Oyama M, Kozuka-Hata H, Sagara H, Kato A, Kawaguchi Y. 2015. Herpes simplex virus 1 recruits CD98 heavy chain and β1 integrin to the nuclear membrane for viral de-envelopment. J Virol 89:7799–7812. https://doi.org/10.1128/JVI.00741-15.
34. Liu Z, Kato A, Oyama M, Kozuka-Hata H, Arii J, Kawaguchi Y. 2015. Role of host cell p32 in herpes simplex virus 1 de-envelopment during viral nuclear egress. J Virol 89:8982–8998. https://doi.org/10.1128/JVI.01220-15.
35. Farnsworth A, Wisner TW, Webb M, Roller R, Cohen G, Eisenberg R, Johnson DC. 2007. Herpes simplex virus glycoproteins gB and gH function in fusion between the virion envelope and the outer nuclear membrane. Proc Natl Acad Sci U S A 104:10187–10192. https://doi.org/10.1073/pnas.0703790104.
36. Mou F, Wills E, Baines JD. 2009. Phosphorylation of the U(L)31 protein of herpes simplex virus 1 by the U(S)3-encoded kinase regulates localization of the nuclear envelopment complex and egress of nucleocapsids. J Virol 83:5181–5191. https://doi.org/10.1128/JVI.00090-09.
37. Shindo K, Kato A, Koyanagi N, Sagara H, Arii J, Kawaguchi Y. 2016. Characterization of a herpes simplex virus 1 (HSV-1) chimera in which the Us3 protein kinase gene is replaced with the HSV-2 Us3 gene. J Virol 90:457–473. https://doi.org/10.1128/JVI.02376-15.
38. Gao J, Finnen RL, Sherry MR, Le Sage V, Banfield BW. 2020. Differentiating the roles of UL16, UL21, and Us3 in the nuclear egress of herpes simplex virus capsids. J Virol 94:e00738-20. https://doi.org/10.1128/JVI.00738-20.
39. Maric M, Shao J, Ryan RJ, Wong CS, Gonzalez-Alegre P, Roller RJ. 2011. A functional role for TorsinA in herpes simplex virus 1 nuclear egress. J Virol 85:9667–9679. https://doi.org/10.1128/JVI.05314-11.
40. Roussel É, Lippé R. 2018. Cellular protein kinase D modulators play a role during multiple steps of herpes simplex virus 1 egress. J Virol 92:e01486-18. https://doi.org/10.1128/JVI.01486-18.
41. Saiz-Ros N, Czapiewski R, Epifano I, Stevenson A, Swanson SK, Dixon CR, Zamora DB, McElwee M, Vijayakrishnan S, Richardson CA, Dong L, Kelly DA, Pytowski L, Goldberg MW, Florens L, Graham SV, Schirmer EC. 2019. Host vesicle fusion protein VAPB contributes to the nuclear egress stage of herpes simplex virus type-1 (HSV-1) replication. Cells 8:120. https://doi.org/10.3390/cells8020120.
42. Leis J, Luan CH, Audia JE, Dunne SF, Heath CM. 2021. Ilaprazole and other novel prazole-based compounds that bind Tsg101 inhibit viral budding of herpes simplex virus 1 and 2 and human immunodeficiency virus from cells. J Virol 95:e00190-21. https://doi.org/10.1128/JVI.00190-21.
43. Wills E, Mou F, Baines JD. 2009. The U(L)31 and U(L)34 gene products of herpes simplex virus 1 are required for optimal localization of viral glycoproteins D and M to the inner nuclear membranes of infected cells. J Virol 83:4800–4809. https://doi.org/10.1128/JVI.02431-08.
44. Milbradt J, Kraut A, Hutterer C, Sonntag E, Schmeiser C, Ferro M, Wagner S, Lenac T, Claus C, Pinkert S, Hamilton ST, Rawlinson WD, Sticht H, Couté Y, Marschall M. 2014. Proteomic analysis of the multimeric nuclear egress complex of human cytomegalovirus. Mol Cell Proteomics 13:2132–2146. https://doi.org/10.1074/mcp.M113.035782.
45. Bahnamiri MM, Roller RJ. 2021. Mechanism of nuclear lamina disruption and the role of pUS3 in HSV-1 nuclear egress. J Virol 95:e02432-20. https://doi.org/10.1128/JVI.02432-20.
46. Reynolds AE, Ryckman BJ, Baines JD, Zhou Y, Liang L, Roller RJ. 2001. U(L)31 and U(L)34 proteins of herpes simplex virus type 1 form a complex that accumulates at the nuclear rim and is required for envelopment of nucleocapsids. J Virol 75:8803–8817. https://doi.org/10.1128/jvi.75.18.8803-8817.2001.
47. Sugimoto K, Uema M, Sagara H, Tanaka M, Sata T, Hashimoto Y, Kawaguchi Y. 2008. Simultaneous tracking of capsid, tegument, and envelope protein localization in living cells infected with triply fluorescent herpes simplex virus 1. J Virol 82:5198–5211. https://doi.org/10.1128/JVI.02681-07.
48. Kato A, Tanaka M, Yamamoto M, Asai R, Sata T, Nishiyama Y, Kawaguchi Y. 2008. Identification of a physiological phosphorylation site of the herpes simplex virus 1-encoded protein kinase Us3 which regulates its optimal catalytic activity in vitro and influences its function in infected cells. J Virol 82:6172–6189. https://doi.org/10.1128/JVI.00044-08.

49. Song Z. 2013. Roles of the nucleotide sugar transporters (SLC35 family) in health and disease. Mol Aspects Med 34:590–600. https://doi.org/10.1016/j.mam.2012.12.004.
50. Orellana A, Moraga C, Araya M, Moreno A. 2016. Overview of nucleotide sugar transporter gene family functions across multiple species. J Mol Biol 428:3150–3165. https://doi.org/10.1016/j.jmb.2016.05.021.
51. Weber AP, Linka N. 2011. Connecting the plastid: transporters of the plastid envelope and their role in linking plastidial with cytosolic metabolism. Annu Rev Plant Biol 62:53–77. https://doi.org/10.1146/annurev-arplant-042110-103903.
52. Lee Y, Nishizawa T, Takemoto M, Kumazaki K, Yamashita K, Hirata K, Minoda A, Nagatoishi S, Tsumoto K, Ishitani R, Nureki O. 2017. Structure of the triose-phosphate/phosphate translocator reveals the basis of substrate specificity. Nat Plants 3:825–832. https://doi.org/10.1038/s41477-017-0022-8.
53. Ryckman BJ, Roller RJ. 2004. Herpes simplex virus type 1 primary envelopment: UL34 protein modification and the US3-UL34 catalytic relationship. J Virol 78:399–412. https://doi.org/10.1128/jvi.78.1.399-412.2004.
54. Perland E, Fredriksson R. 2017. Classification systems of secondary active transporters. Trends Pharmacol Sci 38:305–315. https://doi.org/10.1016/j.tips.2016.11.008.
55. Kandasamy P, Gyimesi G, Kanai Y, Hediger MA. 2018. Amino acid transporters revisited: new views in health and disease. Trends Biochem Sci 43:752–789. https://doi.org/10.1016/j.tibs.2018.05.003.
56. Pizzagalli MD, Bensimon A, Superti-Furga G. 2021. A guide to plasma membrane solute carrier proteins. FEBS J 288:2784–2835. https://doi.org/10.1111/febs.15531.
57. Greenwood AD, Ishida Y, O'Brien SP, Roca AL, Eiden MV. 2018. Transmission, evolution, and endogenization: lessons learned from recent retroviral invasions. Microbiol Mol Biol Rev 82:e00044-17. https://doi.org/10.1128/MMBR.00044-17.
58. Nguyen NNT, Lim YS, Nguyen LP, Tran SC, Luong TTD, Nguyen TTT, Pham HT, Mai HN, Choi JW, Han SS, Hwang SB. 2018. Hepatitis C virus modulates solute carrier family 3 member 2 for viral propagation. Sci Rep 8:15486. https://doi.org/10.1038/s41598-018-33861-6.
59. Ito Y, Komada H, Kusagawa S, Tsurudome M, Matsumura H, Kawano M, Ohta H, Nishio M. 1992. Fusion regulation proteins on the cell surface: isolation and characterization of monoclonal antibodies which enhance giant polykaryocyte formation in Newcastle disease virus-infected cell lines of human origin. J Virol 66:5999–6007. https://doi.org/10.1128/JVI.66.10.5999-6007.1992.
60. Ohta H, Tsurudome M, Matsumura H, Koga Y, Morikawa S, Kawano M, Kusugawa S, Komada H, Nishio M, Ito Y. 1994. Molecular and biological characterization of fusion regulatory proteins (FRPs): anti-FRP mAbs induced HIV-mediated cell fusion via an integrin system. EMBO J 13:2044–2055. https://doi.org/10.1002/j.1460-2075.1994.tb06479.x.
61. Ohgimoto S, Tabata N, Suga S, Nishio M, Ohta H, Tsurudome M, Komada H, Kawano M, Watanabe N, Ito Y. 1995. Molecular characterization of fusion regulatory protein-1 (FRP-1) that induces multinucleated giant cell formation of monocytes and HIV gp160-mediated cell fusion. FRP-1 and 4F2/CD98 are identical molecules. J Immunol 155:3585–3592.
62. Okamoto K, Tsurudome M, Ohgimoto S, Kawano M, Nishio M, Komada H, Ito M, Sakakura Y, Ito Y. 1997. An anti-fusion regulatory protein-1 monoclonal antibody suppresses human parainfluenza virus type 2-induced cell fusion. J Gen Virol 78:83–89. https://doi.org/10.1099/0022-1317-78-1-83.
63. Jahn R, Lang T, Südhof TC. 2003. Membrane fusion. Cell 112:519–533. https://doi.org/10.1016/s0092-8674(03)00112-0.
64. Mondal Roy S, Sarkar M. 2011. Membrane fusion induced by small molecules and ions. J Lipids 2011:528784. https://doi.org/10.1155/2011/528784.
65. Hediger MA, Romero MF, Peng JB, Rolfs A, Takanaga H, Bruford EA. 2004. The ABCs of solute carriers: physiological, pathological and therapeutic implications of human membrane transport proteins. Pflugers Arch 447:465–468. https://doi.org/10.1007/s00424-003-1192-y.
66. Colas C, Ung PM, Schlessinger A. 2016. SLC transporters: structure, function, and drug discovery. Medchemcomm 7:1069–1081. https://doi.org/10.1039/C6MD00005C.
67. Bottger P, Pedersen L. 2002. Two highly conserved glutamate residues critical for type III sodium-dependent phosphate transport revealed by uncoupling transport function from retroviral receptor function. J Biol Chem 277:42741–42747. https://doi.org/10.1074/jbc.M207096200.
68. Kato A, Arii J, Shiratori I, Akashi H, Arase H, Kawaguchi Y. 2009. Herpes simplex virus 1 protein kinase Us3 phosphorylates viral envelope glycoprotein B and regulates its expression on the cell surface. J Virol 83:250–261. https://doi.org/10.1128/JVI.01451-08.
69. Tanaka M, Kagawa H, Yamanashi Y, Sata T, Kawaguchi Y. 2003. Construction of an excisable bacterial artificial chromosome containing a full-length infectious clone of herpes simplex virus type 1: viruses reconstituted from the clone exhibit wild-type properties in vitro and in vivo. J Virol 77:1382–1391. https://doi.org/10.1128/jvi.77.2.1382-1391.2003.
70. Kato A, Adachi S, Kawano S, Takeshima K, Watanabe M, Kitazume S, Sato R, Kusano H, Koyanagi N, Maruzuru Y, Arii J, Hatta T, Natsume T, Kawaguchi Y. 2020. Identification of a herpes simplex virus 1 gene encoding neurovirulence factor by chemical proteomics. Nat Commun 11:4894. https://doi.org/10.1038/s41467-020-18718-9.
71. Tischer BK, von Einem J, Kaufer B, Osterrieder N. 2006. Two-step Red-mediated recombination for versatile high-efficiency markerless DNA manipulation in Escherichia coli. Biotechniques 40:191–197. https://doi.org/10.2144/000112096.
72. Kato A, Tsuda S, Liu Z, Kozuka-Hata H, Oyama M, Kawaguchi Y. 2014. Herpes simplex virus 1 protein kinase Us3 phosphorylates viral dUTPase and regulates its catalytic activity in infected cells. J Virol 88:655–666. https://doi.org/10.1128/JVI.02710-13.
73. Watanabe M, Arii J, Takeshima K, Fukui A, Shimojima M, Kozuka-Hata H, Oyama M, Minamitani T, Yasui T, Kubota Y, Takekawa M, Kosugi I, Maruzuru Y, Koyanagi N, Kato A, Mori Y, Kawaguchi Y. 2021. Prohibitin-1 contributes to cell-to-cell transmission of herpes simplex virus 1 via the MAPK/ERK signaling pathway. J Virol 95:e01413-20. https://doi.org/10.1128/JVI.01413-20.
74. Arii J, Goto H, Suenaga T, Oyama M, Kozuka-Hata H, Imai T, Minowa A, Akashi H, Arase H, Kawaoka Y, Kawaguchi Y. 2010. Non-muscle myosin IIA is a functional entry receptor for herpes simplex virus-1. Nature 467:859–862. https://doi.org/10.1038/nature09420.
75. Kawaguchi Y, Van Sant C, Roizman B. 1997. Herpes simplex virus 1 alpha regulatory protein ICP0 interacts with and stabilizes the cell cycle regulator cyclin D3. J Virol 71:7328–7336. https://doi.org/10.1128/JVI.71.10.7328-7336.1997.
76. Arii J, Takeshima K, Maruzuru Y, Koyanagi N, Kato A, Kawaguchi Y. 2019. Roles of the interhexamer contact site for hexagonal lattice formation of the herpes simplex virus 1 nuclear egress complex in viral primary envelopment and replication. J Virol 93:e00498-19. https://doi.org/10.1128/JVI.00498-19.
77. Morimoto T, Arii J, Tanaka M, Sata T, Akashi H, Yamada M, Nishiyama Y, Uema M, Kawaguchi Y. 2009. Differences in the regulatory and functional effects of the Us3 protein kinase activities of herpes simplex virus 1 and 2. J Virol 83:11624–11634. https://doi.org/10.1128/JVI.00993-09.